Charged-current neutrino-nucleus reactions within the superscaling meson-exchange current approach

G. D. Megias, J. E. Amaro, M. B. Barbaro, J. A. Caballero, T. W. Donnelly, and I. Ruiz Simo

Phys. Rev. D **94**, 093004 — Published 18 November 2016

DOI: 10.1103/PhysRevD.94.093004

Charged-current neutrino-nucleus reactions within the SuSAv2-MEC approach

G.D. Megias,[1] J.E. Amaro,[2] M.B. Barbaro,[3] J.A. Caballero,[1] T.W. Donnelly,[4] and I. Ruiz Simo[2]

[1] *Departamento de Física Atómica, Molecular y Nuclear, Universidad de Sevilla, 41080 Sevilla, Spain*
[2] *Departamento de Física Atómica, Molecular y Nuclear and Instituto Carlos I de Física Teórica y Computacional, Universidad de Granada, 18071 Granada, Spain*
[3] *Dipartimento di Fisica, Università di Torino and INFN, Sezione di Torino, Via P. Giuria 1, 10125 Torino, Italy*
[4] *Center for Theoretical Physics, Laboratory for Nuclear Science and Department of Physics, Massachusetts Institute of Technology, Cambridge, Massachusetts 02139, USA*

We present a detailed study of charged-current (CC) neutrino-nucleus reactions in a fully relativistic framework and comparisons with recent experiments spanning an energy range from hundreds of MeV up to 100 GeV within the SuperScaling Approach, which is based on the analysis of electron-nucleus scattering data and has been recently improved with the inclusion of Relativistic Mean Field theory effects. We also evaluate and discuss the impact of two-particle two-hole meson-exchange currents (2p-2h MEC) on neutrino-nucleus interactions through the analysis of two-particle two-hole axial and vector contributions to weak response functions in a fully relativistic Fermi gas. The results show a fairly good agreement with experimental data over the whole range of neutrino energies.

PACS numbers: 13.15.+g, 25.30.Pt

I. INTRODUCTION

The enormous progress over recent years on neutrino oscillation experiments have motivated many theoretical efforts to achieve a consistent and accurate description of neutrino-nucleus scattering in the GeV region. At these kinematics, several measurements of CC neutrino-nucleus scattering cross sections have been performed by different collaborations (MiniBooNE [1, 2], NOMAD [3], T2K [4–6], SciBooNE [7], MINERνA [8, 9]), revealing the need of describing in a precise way the relevant reaction mechanisms, mainly the quasielastic (QE) regime, one pion production and 2p-2h MEC contributions. In particular, the CCQE MiniBooNE results [1, 2] have stimulated many theoretical studies devoted to explaining the apparent discrepancies between data and most theoretical predictions based on the Impulse Approximation (IA). Based on results from different groups, the inclusion of effects beyond IA, such as multinucleon excitations, mainly 2p-2h MEC contributions, has allowed one to explain these data without including any effective parameter (such as the axial mass M_A) [10–13].

In this context, a consistent evaluation of the (e, e') cross section in the same kinematical regime is crucial for a proper analysis of neutrino-nucleus interactions as it provides a decisive benchmark for assessing the validity of the theoretical description not only in the QE regime, but also for the 2p-2h MEC contributions as well as at higher energy transfers (nucleonic resonances, inelastic spectrum). This has been recently studied in detail in [14], where good agreement with (e, e') data is reached in the framework of the SuperScaling Approach (SuSA) for a wide range of kinematics, covering from the QE regime to the deep inelastic spectrum.

The SuSA approach [15–18] assumes the existence of universal scaling functions for both electromagnetic and weak interactions. Analyses of inclusive (e, e') data have shown that at energy transfers below the QE peak superscaling is fulfilled with very good accuracy [16, 17, 19]: this implies that the reduced cross section exhibits an independence of the momentum transfer (first-kind scaling) and of the nuclear target (second-kind scaling) when expressed as a function of the appropriate scaling variable (ψ), itself a function of the energy (ω) and momentum transfer (q). Nevertheless, at energies above the QE peak both kinds of scaling are violated, which is associated with effects beyond IA, such as 2p-2h MEC or with inelastic contributions. An extension of this formalism, originally introduced to describe the QE regime, to the Δ-resonance domain and the complete inelastic spectrum – resonant, non-resonant and deep inelastic scattering (DIS) – has also been proposed in recent works [20–22] .

Recently we have developed an improved version of the superscaling prescription, called SuSAv2 [23], by incorporating relativistic mean field (RMF) effects [24–26] in the longitudinal and transverse nuclear responses, as well as in the isovector and isoscalar channels. This is of great interest in order to describe CC neutrino reactions that are purely-isovector. Furthermore, a natural enhancement of the transverse nuclear response emerges from the RMF theory as a genuine relativistic effect.

As mentioned before, 2p-2h MEC play an important role in the analysis of neutrino oscillation experiments, being relevant especially in the "dip" region between the QE and the Δ peaks. These are added to our model in the so-called SuSAv2-MEC approach.

Although a comparison of neutrino scattering data with the SuSAv2-MEC predictions was already performed in [27], here two novelties are introduced in the model. The first one concerns the implementation of RMF effects in the SuSA approach. While the RMF works properly at low to intermediate q-values, where the final-state interactions (FSI) between the outgoing nucleon and the residual nucleus are significant, at higher

momentum transfers these effects should become negligible and the Relativistic Plane Wave Impulse Approximation (RPWIA) - where the initial state is described by a mean field but FSI are neglected - is more appropriate to describe the nuclear dynamics in this regime. The pure RMF model fails to reproduce the smooth transition to the RPWIA at high q due to the strong energy-independent scalar and vector potentials included in the model. Hence both approaches are incorporated in the present SuSAv2 model by using a q-dependent blending function, as described in [14], in such a way that the RMF dominates at low and intermediate q-values whereas the RPWIA contributions start to be relevant at higher momentum transfer. The same approach has been applied not only to the QE but also to the inelastic regime and has been shown to provide a successful description of electron-nucleus inclusive data [14] once 2p-2h excitations are also taken into account.

The second new aspect of the present calculation concerns the treatment of 2p-2h excitations. In [27] we used the exact fully relativistic *vector* MEC evaluated in [28, 29]. In this work we include for the first time the fully relativistic weak (with *vector* and *axial* components) charged meson-exchange currents, in both longitudinal and transverse channels. These have been evaluated in [30–32] from an exact microscopic calculation, where the two-body current is the sum of seagull, pion-in-flight, pion-pole and Δ-pole operators and the basis wave functions are non-interacting Dirac spinors.

From this baseline, the SuSAv2-MEC predictions can be employed for the analysis of neutrino-nucleus reactions covering the entire energy spectrum once all the inelastic channels, already included for electron scattering, are also incorporated for neutrino reactions. This is presently in progress and results will be presented in a forthcoming publication. In this work we restrict ourselves to the contribution ascribed to the Δ-resonance that in most of the cases plays a major role.

This paper is organized as follows. In Sect. II we briefly introduce the formalism for CCQE neutrino-nucleus scattering and describe our 2p-2h MEC calculations. In Sect. III we present a comparison of our QE and 2p-2h MEC predictions with all recent CCQE neutrino experimental data. An extension to the analysis of inclusive neutrino cross sections is shown in Sect. IV. Finally, in Sect. V we draw the conclusions of our study, including some remarks related to further work.

II. THEORETICAL FORMALISM

The general formalism describing CC neutrino-nucleus scattering has been detailed in previous works [15, 33], where the double differential (ν_l, l') cross section is given as the sum of longitudinal (L) and transverse (T) channels, each of them composed of pure vector (VV) and axial components (AA), and the interference transverse (T') vector-axial channel (VA), which is constructive (+) for neutrino scattering and destructive (-) for antineutrino one:

$$\frac{d\sigma}{dk'd\Omega} = \sigma_0 \left(\hat{V}_L R_L + \hat{V}_T R_T \pm 2\hat{V}_{T'} R_{T'} \right) , \qquad (1)$$

where

$$\hat{V}_L R_L = \hat{V}_{CC} R_{CC} + 2\,\hat{V}_{CL} R_{CL} + \hat{V}_{LL} R_{LL} \,, \qquad (2)$$

R_K are the nuclear response functions and

$$\sigma_0 = \frac{G_F^2 \cos^2\theta_c}{2\pi^2} \left(k' \cos\frac{\tilde{\theta}}{2} \right)^2 \qquad (3)$$

depends on the Fermi constant G_F, the Cabibbo angle θ_c, the outgoing lepton momentum k', and the generalized scattering angle $\tilde{\theta}$.

The terms $\hat{V}_K$ are kinematical factors whose explicit expressions are

$$\hat{V}_{CC} = 1 - \delta^2 \tan^2\frac{\tilde{\theta}}{2} \qquad (4)$$

$$\hat{V}_{CL} = \frac{\omega}{q} + \frac{\delta^2}{\rho'} \tan^2\frac{\tilde{\theta}}{2} \qquad (5)$$

$$\hat{V}_{LL} = \frac{\omega^2}{q^2} + \left(1 + \frac{2\omega}{q\rho'} + \rho\delta^2 \right) \delta^2 \tan^2\frac{\tilde{\theta}}{2} \qquad (6)$$

$$\hat{V}_T = \tan^2\frac{\tilde{\theta}}{2} + \frac{\rho}{2} - \frac{\delta^2}{\rho'} \left(\frac{\omega}{q} + \frac{1}{2}\rho\rho'\delta^2 \right) \tan^2\frac{\tilde{\theta}}{2} \qquad (7)$$

$$\hat{V}_{T'} = \frac{1}{\rho'} \left(1 - \frac{\omega\rho'}{q}\delta^2 \right) \tan^2\frac{\tilde{\theta}}{2} \,. \qquad (8)$$

In Eqs. (4–8) we have defined

$$\delta = \frac{m_l}{\sqrt{|Q^2|}} \qquad (9)$$

$$\rho = \frac{|Q^2|}{q^2} \qquad (10)$$

$$\rho' = \frac{q}{\epsilon + \epsilon'} \,, \qquad (11)$$

where m_l is the final charged lepton mass.

As anticipated in the Introduction, in this work we evaluate the nuclear responses by employing a set of purely isovector scaling functions based on the RMF and the RPWIA models (SuSAv2 model) in order to account properly the FSI between the outgoing nucleon and the residual nucleus, as described in [14, 23]. Contrary to the original SuSA approach that makes use of a single-universal scaling function extracted from the analysis of the longitudinal response function for electron scattering, the new SuSAv2 incorporates more degrees of freedom by employing also an enhanced transverse scaling function that is consistent with the theoretical predictions provided by the RMF. Moreover, the SuSAv2 model applied to neutrino reactions takes into account purely isovector contributions. The RMF has proved its capability to describe with a high precision the behavior

of quasielastic electron scattering data. It is one of the few theoretical models based on the impulse approximation that produces an asymmetrical longitudinal scaling function, with a tail extended to large transferred energies, in accordance with data. Furthermore, it also provides a significant enhancement in the transverse scaling function, a genuine dynamical relativistic effect, that is also supported by the analysis of data. This, in addition to the pure isovector character of the neutrino scaling functions, makes SuSAv2 much more reliable than the original SuSA. However, the RMF model, in spite of its success at low-intermediate energies, fails at high q-kinematics. The strong energy-independent scalar and vector potentials involved within the RMF lead to a too repulsive final state interaction for the ejected nucleon. This shortcoming of the model is corrected by constructing a general scaling function that takes care of the main properties of the RMF model at low-intermediate q-values, whereas it behaves following the RPWIA results at higher q. Although this procedure introduces new free parameters, its validity has been clearly tested for very different kinematical situations [14], and it has been applied not only to the QE region but also to the inelastic one, i.e., the same general scaling function is used for the two very different regimes. Details on the parameterizations of the SuSAv2 scaling functions are reported in the Appendix.

A comment is in order concerning the gauge invariance of the model which is at some level broken. However, it is important to point out that any theoretical description of electron (neutrino)-nucleus processes based on the impulse approximation breaks gauge invariance and/or current conservation, even when using the same potential to describe the initial and final nucleon states. This is a consequence of the assumptions in the impulse approximation and the lack of knowledge on how to describe the current operator for a bound/distorted nucleon wave function. In the case of the RMF we have checked that the use of the so-called CC2 nucleon current operator [25] leads to an almost gauge invariant result. Within RPWIA gauge uncertainties are very minor. Therefore, SuSAv2 is fully based on RMF/RPWIA-CC2 results.

Concerning the description of the 2p-2h MEC, we employ a calculation performed within the relativistic Fermi gas model in which a fully Lorentz covariant analysis can be achieved [30, 31]. In the present study we include for the first time the axial contribution in both longitudinal and transverse channels.

As it has been analyzed in previous works, a fully relativistic calculation of the 2p-2h MEC response functions involves a non-trivial calculation of all the many-body MEC diagrams, which implies more than 100,000 terms and subsequent seven-dimensional integrations. To reduce the computational time as well as to ease the implementation of the model in MonteCarlo generators used in the analysis of current neutrino oscillation experiments, where a broad range of kinematics are involved, we make use of a parametrization of the MEC responses. The functional form employed for the parametrization of the transverse electromagnetic vector response was detailed in [27]. In the present work, we follow this prescription and extend it to the different axial and vector components involved in the analysis of CC neutrino reactions as well as considering both transverse and longitudinal contributions.

Finally, we consider an extension of the SuSAv2 model to the region where the Δ-excitation dominates, as presented in [22]. This approach has been carried out by subtracting the QE+MEC contribution from the experimental (e, e') cross section in a similar way as done in the SuperScaling model for the QE regime. Therefore, we obtain a new scaling function f^{Δ} which is suited to the Δ-resonance region and can be applied to analyze inclusive neutrino-nucleus cross sections, such as recent results from the T2K and SciBooNE collaborations. We are aware that other higher nucleon resonances, that may have a significant role for some particular kinematics in the inelastic regime, are not taken into account, and moreover, the resulting Δ scaling function differs from the one used within the SuSAv2. We show that the pure Δ response, as we have evaluated it, does provide the most significant contribution in some kinematical situations like the T2K experiment. This is consistent with the results presented in [22] where it is shown that the Δ contribution at ψ_{Δ} values above 0.5 is almost negligible for the T2K cross section. This kinematical region is related to high momentum transfers where other resonances and deep inelastic scattering processes are relevant. Our interest in the near future is to extend SuSAv2 to the inelastic neutrino region by using the same scaling function as in the QE domain, just as done for electron scattering reactions [14]. This requires the description of the weak inelastic neutrino-nucleon response functions, a project still in progress.

A. 2p-2h MEC responses

In this section we illustrate and discuss in detail some properties of the 2p-2h MEC response functions. Before entering into a detailed discussion of the results, let us remind that 2p2h MEC calculations are linked to the Fermi Gas Model, whereas the SuSAv2 approach emerges from the original calculations based on the RMF model. The main justification for this hybrid approach resides in the technical difficulties inherent to the calculation of such contributions, which as already stressed is extremely cumbersome even in the simple RFG basis. It is worth pointing out that most of calculations in the literature [34–37] are based also on the Fermi gas model. One of the few approaches that, to our knowledge, use realistic nuclear wave functions is the one of [38, 39] which is however non-relativistic and implies an enormous computational effort, difficult to apply to the extended kinematics involved in neutrino experiments. On the other hand, the 2p-2h calculations in the shell model by [40]

were in agreement with the findings of [35].

In Fig. 1 we compare the contributions of the different 2p-2h MEC responses as functions of the energy transferred to the nucleus for two values of the momentum transfer, q=600 and 1000 MeV/c. Note that in general the 5 responses are comparable in size, depending on the specific kinematics. However, in the cross section the contribution of the CC and LL is roughly compensated by that of the negative CL response, so that for neutrino energies below ~ 1 GeV the net longitudinal contribution plays a minor role in the total MEC response. This is illustrated in Fig. 2, where the L, T and T' contributions to the 2p-2h MEC cross section are displayed versus the neutrino energy. At higher energies the L and T' contributions become comparable, both being much smaller that the dominant T one.

The balance between the longitudinal and transverse 2p-2h channel discussed above is somehow different from the one emerging in the electromagnetic case. As described in a recent work [14], the longitudinal electromagnetic MEC response is indeed negligible with regard to the transverse one. However, as illustrated in Fig. 2b, we notice that when computing the total 2p-2h MEC weak cross section the longitudinal contribution is dominated by the axial channel and thus it plays a more relevant role compared with the EM case.

Concerning the transverse responses, it is noticeable that the magnitude of the pure axial and vector channels to the cross section are very similar. Moreover, the vector-axial interference contribution reaches its maximum around $E_\nu \sim$1 GeV and decreases at higher energies as a consequence of the behavior of the leptonic factor $V_{T'}$.

The analysis of the evolution with q of the individual transverse components (see Fig. 3) shows that the axial term is larger than the vector one at low-intermediate kinematics ($q < 800$ MeV/c) whereas the opposite occurs at higher kinematics.

To conclude this section, it is also important to identify the kinematical region where the 2p-2h MEC responses attain their maximum values. This is clearly illustrated in the density plot of Fig. 4, which represents the double differential cross section in terms of ω and q at $E_\nu = 3.0$ GeV; here the top (bottom) panel corresponds to the 2p-2h MEC (pure QE) contributions. As shown in the figure, the main contribution to the MEC cross section comes from $q \in (0.3, 1.0)$ GeV/c and $\omega \in (0.3, 0.8)$ GeV. On the contrary, the QE peak is moved to lower values of ω. Both the one-body and two-body responses die with the momentum transfer q, but their ratio is rather constant (see [31]). Although results in Fig. 4 correspond to a fixed incident neutrino energy, 3 GeV, similar results are obtained for larger E_ν values. It is important to point out the differences between our predictions and those ones based on the model of Nieves [41] that show the 2p-2h MEC contribution to be shifted to slightly bigger values of the energy and momentum transfer. For completeness we also show in Fig. 5 the density plots for the 2p-2h MEC contributions in terms of the values of the muon kinetic energy and the scattering angle for three values of neutrino energy: 1 GeV (top panel), 3 GeV (middle) and 10 GeV (bottom). As observed, the main contribution resides in the region of very small angles, close to zero.

III. RESULTS

In this section we show the predictions of the SuSAv2-MEC model compared with data from different collaborations: MiniBooNE, MINERνA, T2K and SciBooNE. Our study is mainly restricted to the quasielastic (QE) regime where the impulse approximation in addition to the effects linked to the 2p-2h meson-exchange currents play a major role. However, some results that incorporate the contribution of the Δ excitation are also compared with data. As shown in [14] the SuSAv2-MEC model has been applied to the inelastic region for electron scattering. Its extension to neutrino reactions is in progress and their predictions will be shown in a forthcoming publication. However, the resonant pion production, that in most cases is the largest contribution, is computed following our previous investigations in [22]. It is worth pointing out that those diagrams that correspond to the excitation of a 2p2h+π state, hence to pion production [42], are implicitly included in the phenomenological inelastic scaling function. Notice that in the particular case of neutrino reactions, the inelastic regime only incorporates the contribution of the Δ excitation. Hence caution should be drawn on the analysis of results corresponding to energies where high inelasticities can play a significant role. As it will be shown in Section III.B, this is the case of the CC inclusive SciBooNE experiment where the Δ contribution is not enough and new channels are needed to explain the data.

In the case of the QE regime, our study includes the analysis of neutrino and antineutrino scattering reactions corresponding to MiniBooNE as well as to MINERνA experiments. In the latter we consider muon and electron neutrinos. Results for T2K are also analyzed in detail. In this case, in order to make the discussion that follows simpler, we first restrict ourselves to the QE domain, and we extend the discussion later to inclusive charged-current (CC) neutrino reactions where high inelasticities are of significance. Our main interest is to show the capability of the present model, SuSAv2-MEC, to describe successfully a large variety of neutrino scattering data corresponding to different experiments with a wide range of kinematics explored. The model, that was already proven to be capable of reproducing (e, e') data, is now extended to neutrinos with emphasis on the crucial role played by 2p-2h MEC effects. These have been computed for the first time within a fully relativistic formalism and without resorting to any particular assumption on the different responses: vector-vector, axial-axial and vector-axial interference.

A. CCQE experimental cross sections

In Figs. 6 – 9 we show the double differential cross section averaged over the neutrino (antineutrino) energy flux against the kinetic energy of the final muon. Figs. 6, 7 (Figs. 8, 9) correspond to neutrino (antineutrino) scattering on ^{12}C. Data are taken from the MiniBooNE collaboration [1, 2]. We represent a large variety of kinematical situations where each panel refers to results averaged over a particular muon angular bin. Notice that the mean energy of the MiniBooNE ν_μ ($\overline{\nu}_\mu$) flux is 788 (665) MeV. These high energies require a fully relativistic treatment of the process. In Figs. 6 – 9 we show results for the pure QE response (red dot-dashed line), the total contribution of the 2p-2h MEC (orange dashed line), *i.e.,* including vector and axial terms in the three responses, L, T and T'. Finally, the total response (QE+2p-2h MEC) is represented by the solid blue line.

As observed, the model tends to overpredict the data for the most forward angles, *i.e.,* $0.9 \leq \cos\theta_\mu \leq 1$. This corresponds to very small energy and momentum transfers, a kinematic situation where "quasi-free" scattering is highly questionable. However, note how well the pure QE response fits the data, in particular, for neutrinos. As the scattering angle increases, the theoretical prediction including both the QE and the 2p-2h MEC effects agrees well with the data. This is the case for neutrinos and antineutrinos (Fig. 6 and Fig. 8) at angles below 90 deg. On the contrary, the discrepancy between theory and data tends to increase as θ_μ gets larger (Figs. 7 and 9). Notice, however, that in these situations only a small number of data points with large uncertainties exist and the cross section is much smaller. Results in Figs. 6 – 9 clearly show the relevant role played by effects beyond the impulse approximation. In particular, 2p-2h MEC contributions are essential in order to describe data. Their relative percentage at the maximum, compared with the pure QE response, being of order $25-35\%$. The relative strength associated with 2p-2h MEC gets larger for increasing values of the angle, particularly, in the case of antineutrinos. Note that, in spite of the quite different neutrino and antineutrino energy fluxes, the quality of the agreement with data is rather similar in the two cases.

The important role of 2p2h excitations to describe these data has been discussed at length in previous works [10, 34, 43] but using different kinds of non-relativistic approximations and some assumptions on the behavior of the responses entering in neutrino reactions, *i.e.,* assuming the axial-axial contributions being equal to the vector-vector ones and the interference T' response to be proportional to the pure transverse vector-vector one. Here we calculate explicitly all the contributions within a fully relativistic framework. To illustrate this point we present in Fig. 10 the separate 2p-2h MEC contributions to the different channels (L, T_{VV}, T_{AA} and T'_{VA}) corresponding to the MiniBooNE double differential cross section at different bins of the muon scattering angle. Results in Fig. 10 show that the T_{AA} and T_{VV} contributions are different, the latter being shifted to higher T_μ values by about 50 MeV for all angular bins. At very forward angles, i.e., lower q-values, the global magnitude of the AA channel is greater than the VV one, in accordance with the results observed in Fig. 3. Concerning the interference T'_{VA} component, its magnitude is not so different from the VV and AA ones at very forward angles, being on the contrary the most relevant contribution at larger angles. Finally, although the longitudinal channel gives the smallest global contribution, its role is essential in order to interpret antineutrino scattering at backward angles. This is a consequence of the negative T'_{VA} term that almost cancels out the $T_{VV}+T_{AA}$ contribution. Fig. 3 also shows clearly that at q of the order of 400 MeV/c the T_{VV} and T_{AA} responses differ by a factor 2 at the maximum. This difference decreases for higher q-values.

To complete the previous discussion on the double differential cross sections, we present in Figs. 11 and 12 the results averaged over the muon kinetic energy bins as functions of the muon scattering angle for neutrinos and antineutrinos, respectively. These graphs complement the previous ones, and prove the capability of the model to reproduce the data for a large variety of kinematic situations. The 2p-2h MEC contributions increase the pure QE response by $\sim 25-35\%$ (depending on the particular region explored) and are shown to be essential in order to describe the data. As observed, the total model tends to overpredict the data measured at angles close to zero and T_μ in the vicinity of $\sim 0.8-1$ GeV. This is consistent with results in previous figures and the inability of the model to describe properly data at very small angles. However, the largest discrepancy between theory and data occurs at the smallest muon kinetic energy bins considered, *i.e.,* $0.2 < T_\mu < 0.4$, in particular, for neutrinos (Fig. 11) and angles bigger than 90^0 ($\cos\theta_\mu < 0$). As seen, the data are higher by $\sim 25-30\%$ than theoretical predictions. This outcome is consistent with the partial results shown in the panels on the bottom in Figs. 6 and 8.

In Fig. 13 results are presented for the MiniBooNE flux averaged CCQE $\nu_\mu(\overline{\nu}_\mu)-^{12}$C differential cross section per nucleon as a function of the muon scattering angle (top panels) and the muon kinetic energy (bottom panels). The integration over the muon kinetic energy has been performed in the range 0.2 GeV $< T_\mu <$ 2.0 GeV. Panels on the left (right) correspond to neutrinos (antineutrinos). As shown, and in consistency with previous results, the SuSAv2-MEC model is capable of reproducing the magnitude as well as the shape of the experimental cross section in all of the cases. For completeness, we also show in Fig. 14 the total flux-unfolded integrated cross section per nucleon versus the neutrino (left panel) and antineutrino (right) energies. The energy range has been extended to 100 GeV and data are shown for the MiniBooNE and NOMAD experiments. Whereas 2p-2h MEC contributions are needed in order to repro-

duce MiniBooNE data (in consistency with the discussion applied to previous figures), the NOMAD experiment seems to be in accordance with the pure QE response. As observed, the role of 2p-2h MEC is very significant at all neutrino (antineutrino) energies, getting an almost constant value for E_ν ($E_{\overline{\nu}}$) greater than $1-2$ GeV. At these values the pure QE cross section is increased by $\sim 30-35\%$ due to 2p-2h MEC. It is important to point out that, in spite of the very large neutrino (antineutrino) energies involved in NOMAD experiment, the main contribution to the cross section, about $\sim 90\%$, comes from momentum and energy transfers below ~ 1 GeV/c and ~ 0.5 GeV, respectively.

The results in Fig. 15 correspond to the MINERνA flux averaged CCQE $\nu_\mu(\overline{\nu}_\mu)$ differential cross section per nucleon as a function of the reconstructed four-momentum Q^2_{QE} (see [44] for details). The top panel refers to $\nu_\mu-^{12}$C whereas the bottom panel contains predictions and data for $\overline{\nu}_\mu-$CH. The mean energy of the MINERνA flux is much higher than the MiniBooNE one, about 3 GeV for both ν_μ and $\overline{\nu}_\mu$. As observed, significant contributions of the 2p-2h MEC, of the order of $\sim 35-40\%$ ($\sim 25\%$) at the maxima for ν_μ ($\overline{\nu}_\mu$), are needed in order to reproduce the experimental data that correspond to a new analysis performed by the MINERνA collaboration [44]. These data exceed by $\sim 20\%$ the ones already presented in previous publications [8, 9] that, on the other hand, were consistent with calculations based exclusively on the impulse approximation (see [46]). Thus, the new MINERνA analysis shows its consistency with the MiniBooNE data. In spite of the very different muon neutrino (antineutrino) energy fluxes in the two experiments, 2p-2h MEC effects remain very significant (on average, $25-35\%$) being their contribution essential in order to fit the data.

Similar comments apply to the case of electron neutrinos [45]. In Fig. 16 we present the MINERνA flux averaged CCQE ν_e differential cross section per nucleon as a function of the electron energy (top-left panel), electron angle (top-right) and reconstructed four-momentum (bottom-left). Compared to the muon neutrino (antineutrino) fluxes, the ν_e and $\overline{\nu}_e$ ones have roughly the same shape in the region of the peak but the tail region is significantly higher in the electronic case. In all of the situations, results are shown for the pure QE response based on the IA (black line), the 2p-2h MEC contribution (orange dashed line) and the total response (blue dot-dashed). In all the cases the contribution at the maximum coming from the 2p-2h MEC is roughly $30-35\%$ compared with the pure QE response. These results are similar to the ones already presented for muon neutrinos (antineutrinos), and they show the importance of 2p-2h effects in order to explain the behavior of data. As observed, the model is capable of reproducing successfully the data. For completeness, we present in the right-bottom panel the results corresponding to the ratio between the flux averaged CCQE $\nu_e+\overline{\nu}_e$ and ν_μ cross sections versus the reconstructed four-momentum. We compare the predictions of the model (red curve) with the data. However, the large error bars presented by the data make this particular analysis rather questionable.

In Fig. 17 we present the flux-averaged double differential cross sections corresponding to the T2K experiment [6]. The graphs are plotted against the muon momentum, and each panel corresponds to a bin in the scattering angle. As in previous cases, we show the separate contributions of the pure QE, the 2p-2h MEC and the sum of both. Contrary to the MiniBooNE and MINERνA experiments, the T2K data show a larger dispersion with significant error bands. Concerning the theoretical predictions, in the present case the relative contribution of the 2p-2h MEC compared with the pure QE is significantly smaller than in the previous cases; of the order of $\sim 10\%$ at the maximum of the peak. This can be connected with the T2K neutrino flux that, although with an averaged neutrino flux similar to MiniBooNE, shows a much narrower distribution. Hence 2p-2h MEC contribute less to the differential cross section.

As observed, the theoretical model is capable of reproducing the data although, contrary to the previous experiments, the addition of the 2p-2h MEC does not seem to improve in a clear way the comparison with data. Due to the large error bands and great dispersion shown by T2K data in most of the kinematical situations, both the pure QE as well as the total, QE+2p-2h MEC, predictions are in accordance with the experiment. It is interesting to point out the results for the most forward angles, *i.e.,* the panel on the right-bottom corner. Notice that the QE and 2p-2h MEC contributions are stabilized to values different from zero for increasing muon momenta as a consequence of the high energy tail of the T2K neutrino flux. This is at variance with all remaining situations where the cross sections decrease significantly as the muon momentum p_μ goes up.

To conclude this Section, we would like to stress that the SuSA approach consists in extracting a phenomenological scaling function from QE electron scattering data. This function implicitly contains all the nuclear dynamics relevant in the scaling regime, including mean field effects, long- and short-range correlations, etc., up to scaling violations that the analysis of experimental data has shown to be small. The microscopic content of the scaling function can be studied using different theoretical approaches. We have offered one possible explanation in terms of relativistic mean field theory, where correlations are not explicitly present, although they might be effectively accounted for to some extent. The RMF gives a remarkably good representation of the data: it fulfills the observed scaling properties and it yields a scaling function whose size and shape agree with the data. However, when compared to neutrino scattering data, other theoretical approches, quite different from the RMF, also provide a similar agreement. For example, long-range RPA correlations have been claimed to play a crucial role in the QEP regime by both the Valencia [12] and Lyon [34] groups. On the other hand a recent calculation of the Ghent group [47] arrives at quite different conclusions,

finding that the CRPA cross sections are very similar to the Hartree-Fock ones. In fact, the result of RPA calculations strongly depends on the microscopic NN interaction, which is phenomenological and fitted to a specific kinematical regime.

Although RPA correlations are not explicitly included in our model, they might be implicitly contained in the superscaling function, which was originally fitted to the data [15–18] precisely to account for all nuclear effects not included in the single nucleon responses. In the SuSA approach their role cannot be disentangled from other nuclear effects, but it must be consistent with the observed superscaling properties of (e, e') data. A comparison of microscopic RPA calculations with the experimental scaling data and its validation against the global set of (e, e') data would be very helpful in order to clarify this issue.

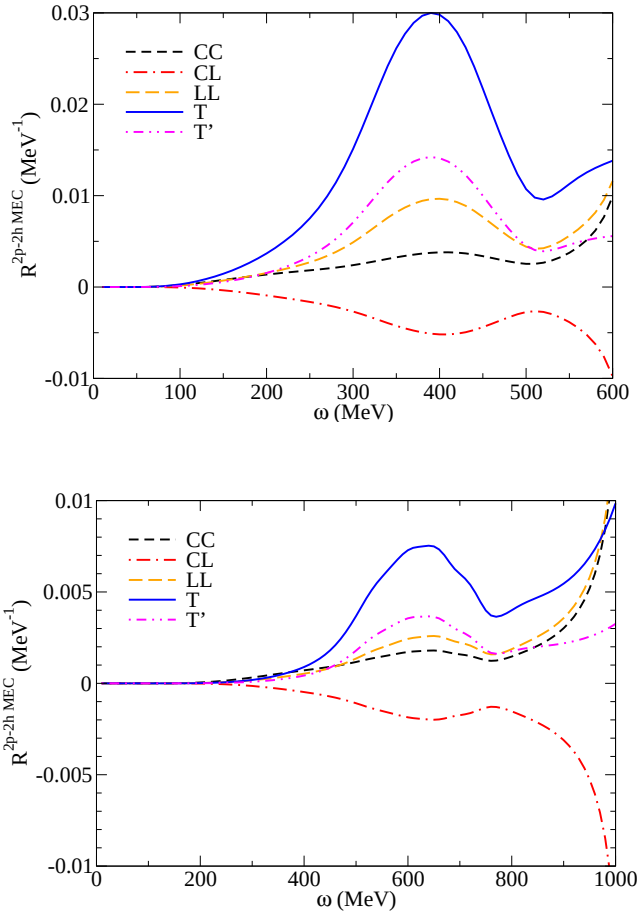

FIG. 1. (Color online) Comparison between 2p-2h MEC transverse ($T = T_{VV} + T_{AA}$ and $T' = T'_{VA}$) response functions and the longitudinal ones (CC, CL and LL) at $q = 600$ MeV/c (top panel) and $q = 1000$ MeV/c (bottom panel).

B. Inclusive ν-^{12}C cross sections

The whole analysis presented in the previous section has been restricted to the case of CCQE cross sections, *i.e.,* only considering the contributions coming from the pure QE peak and the 2p-2h MEC effects. Here we extend our study by including the inelastic contributions. We restrict our discussion to the effects associated with the Δ resonance. The analysis of higher inelasticities is still in progress and it will be presented in a forthcoming publication. The addition of inelastic channels is essential in order to explain inclusive charged-current neutrino cross sections. This is the case of recent data taken by the T2K collaboration [4, 5], both for muon and electron neutrinos, as well as the SciBooNE experiment [7].

Fig. 18 contains the data and theoretical predictions corresponding to the T2K flux-averaged inclusive double differential cross sections for muon neutrinos. Results are shown as function of the muon momentum and averaged over particular muon angular bins (each panel). The separate contribution of the QE (solid blue line), 2p-2h MEC (dashed red) and the Δ resonance (brown band) are presented. The global response is shown by the green band. The band in the pion contribution takes care of the uncertainty associated with the description of the Δ scaling function as discussed in detail in [22]. As observed, the model provides a very nice description of data once all contributions are included, *i.e.,* QE, 2p-2h MEC and pion. This is consistent with the kinematics implied by the present T2K experiment being the Δ resonance the main response (almost the only one) within the inelastic region. This was already discussed in detail in [22] where a similar figure was presented, although based on the original SuSA model and with incomplete 2p-2h MEC calculations. The main difference between the two calculations is the inclusion, in the new results, of the axial 2p-2h contribution. Whereas in [22] the purely vector MEC were found to be negligible at these kinematics, in Fig. 18 it is shown that the axial two-body currents give a contribution almost as large as the one associated with the Δ resonance. The experimental error bars are too large to allow one to discriminate between the two results and both calculations are compatible with the data.

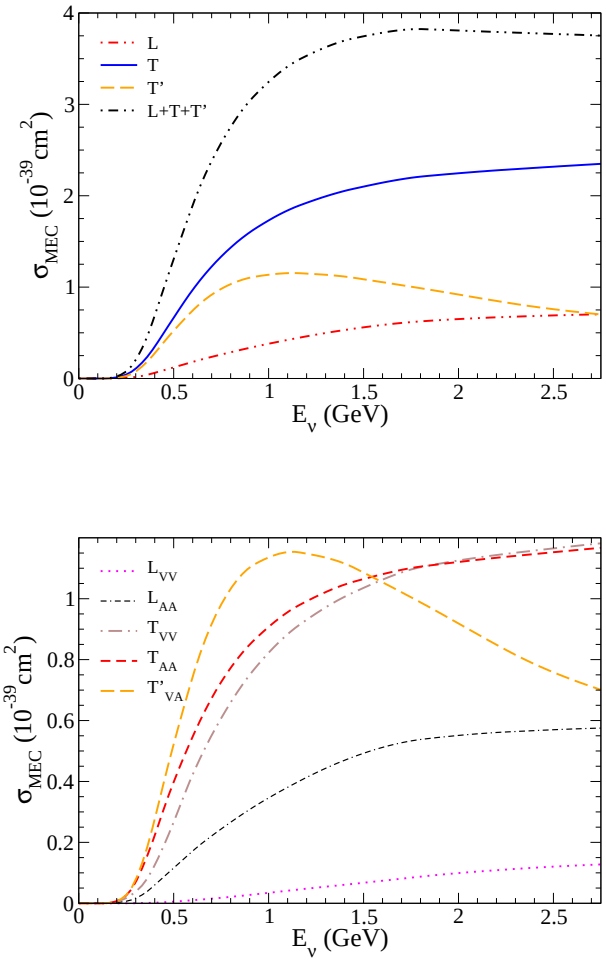

FIG. 2. (Color online) Separation into components of the total 2p-2h MEC ν_μ cross section displayed versus neutrino energy E_ν. The total longitudinal (L), transverse (T) and transverse interference (T') contributions are shown (top panel) as well as the total 2p-2h MEC cross section ($L+T+T'$). Longitudinal and transverse channels are decomposed into vector and axial contributions (bottom panel).

The inclusive T2K experiment for electron neutrinos is analyzed in Fig. 19 where the flux-averaged single differential cross sections are shown. Results are presented against the electron scattering angle (top panel), the electron momentum (middle) and the reconstructed four-momentum (bottom). In the three cases we show the separate contributions corresponding to the QE response (blue line), the 2p-2h MEC (red dashed), pionic (brown band) and the total response (green region). Although, as noted, the role associated with the Δ resonance is essential, the data are located above the model predictions. This implies that other higher nucleon resonances, not taken into account in the present description, may also have a significant role in explaining T2K ν_e data. This is particularly true for increasing values of the electron momentum (see results in the middle panel) and/or the reconstructed four-momentum transfer (bottom panel). Work along this line is presently in progress.

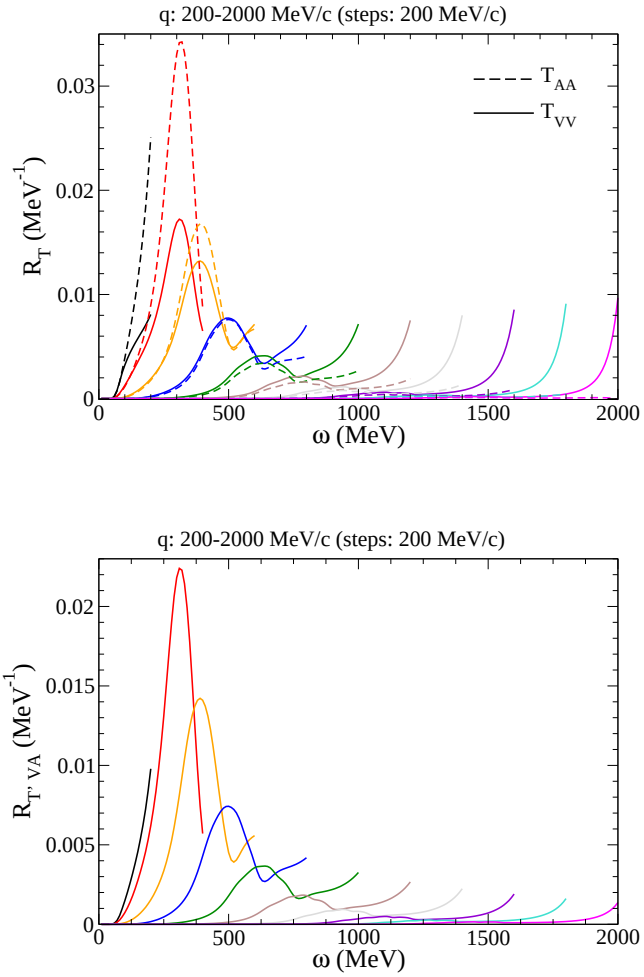

FIG. 3. (Color online) Comparison between 2p-2h MEC axial-axial transverse (T_{AA}) response functions and the vector-vector ones (T_{VV}) versus ω (top panel). The transverse vector-axial interference term (T'_{VA}) is also shown (bottom panel). The curves are displayed from left to right in steps of $q = 200$ MeV/c.

To conclude, we present in Fig. 20 the results for the SciBooNE experiment [7]. These correspond to CC ν_μ ($\overline{\nu}_\mu$) scattering on a polystyrene target. The data are presented as a total unfolded integrated cross section as a function of the neutrino energy. Because of the unfolding procedure to reconstruct the neutrino energy, one should be very cautious in the comparison between data and theoretical predictions (see discussion in [7]). The case of neutrinos is presented in the left panel of Fig. 20 in comparison with available data, whereas the predicted cross section for antineutrinos is referred to the right panel. Results in Fig. 20 are similar to the ones shown in Fig. 7 of [22], although there the 2p-2h MEC calculation only included the pure vector contributions. In fact, one can observe how the complete 2p-2h MEC calculation, now including also the axial currents, leads to a much more significant contribution, bringing the global predictions closer to the data. Contrary to the analysis in [22], here the model reproduces the neutrino data up to 1 GeV. However, for higher energies the model still underpredicts the data by a significant amount. This result clearly indicates that new channels and higher nucleon resonances, in addition to the resonant pion production, should be added to the model. Finally, for completeness, we also show the results obtained for electron antineutrinos with the separate contributions of the different channels. Notice that the role ascribed to the 2p-2h MEC effects is of the order of $\sim 15\%$ ($\sim 20\%$) for neutrinos (antineutrinos), approximately twice compared with the values discussed in [22].

Before concluding we would like to make contact with the recent work based on the Giessen-Boltzmann-Uehling-Uhlenbeck (GiBUU) model that incorporates 2p2h interactions [48]. The calculation makes use of several assumptions based on electron scattering data and the specific contribution of the separate channels. In particular, the 2p2h contributions are assumed to be purely transverse so all electron, neutrino and antineutrino cross sections are expressed in terms of one single structure function that is given by a simple parameterization. The model also gives a good description of electron and neutrino data.

IV. CONCLUSIONS

We have performed a joint calculation of quasielastic and 2p-2h contribution to neutrino and antineutrino scattering cross sections in ^{12}C, using the SuSAv2 model for the quasielastic responses and the relativistic Fermi gas model for the 2p-2h meson exchange currents in the weak sector. The model has been validated in the vector sector by describing the full set of inclusive electron scattering ^{12}C data. We have analyzed the published data from the experiments MiniBooNE, T2K, MINERvA, NOMAD and SciBooNE, spanning a wide range of neutrino energies from hundreds of MeV to hundreds of GeV. For comparison with inclusive data we have used an extension of the SuSAv2 model to the Δ production region to model resonant pion production. We find that the 2p-2h channel is large, contributing about 15–25% depending on the kinematics, and it is essential to describe a great amount of experimental data.

This model is a promising candidate for analyzing the forthcoming neutrino experiments; work is in progress to extend it to higher inelasticities, to provide the separate charge channel contributions, pn, pp and nn emission [49], and to describe the cross section of asymmetric nuclei ($Z \neq N$).

ACKNOWLEDGMENTS

This work was supported by Spanish Direccion General de Investigacion Cientifica y Tecnica and FEDER funds (grants No. FIS2014-59386-P and No. FIS2014-53448-C2-1), by the Agencia de Innovacion y Desarrollo de Andalucia (grants No. FQM225, FQM160), by INFN under project MANYBODY, and part (TWD) by U.S. Department of Energy under cooperative agreement DE-FC02-94ER40818. GDM acknowledges support from a Junta de Andalucia fellowship (FQM7632, Proyectos de Excelencia 2011). IRS acknowledges support from a Juan de la Cierva fellowship from Spanish MINECO.

Appendix A: Parametrization of the charged-current neutrino and antineutrino scaling functions

In this Appendix we summarize the parametrization of the reference scaling functions. The RMF scaling functions are given in terms of a skewed-Gumbel (sG) function, defined as

$$\tilde{f}_{sG} = S(\nu_0;\psi) f_G(\psi_0,\sigma,\beta;\psi)\,, \tag{A1}$$

where

$$S(\nu_0;\psi) = \frac{2}{1+e^{\nu/\nu_0}} \tag{A2}$$

$$f_G(\psi_0,\sigma,\beta;\psi) = \frac{\beta}{\sigma} e^{\nu} \exp[-e^{\nu}] \tag{A3}$$

$$\nu = -\left(\frac{\psi-\psi_0}{\sigma}\right). \tag{A4}$$

In Table I, the values of the free parameters that fit the corresponding longitudinal (L) and transverse (T) RMF scaling functions are shown. The differences linked to the isospin effects (τ) are also taken into acccount.

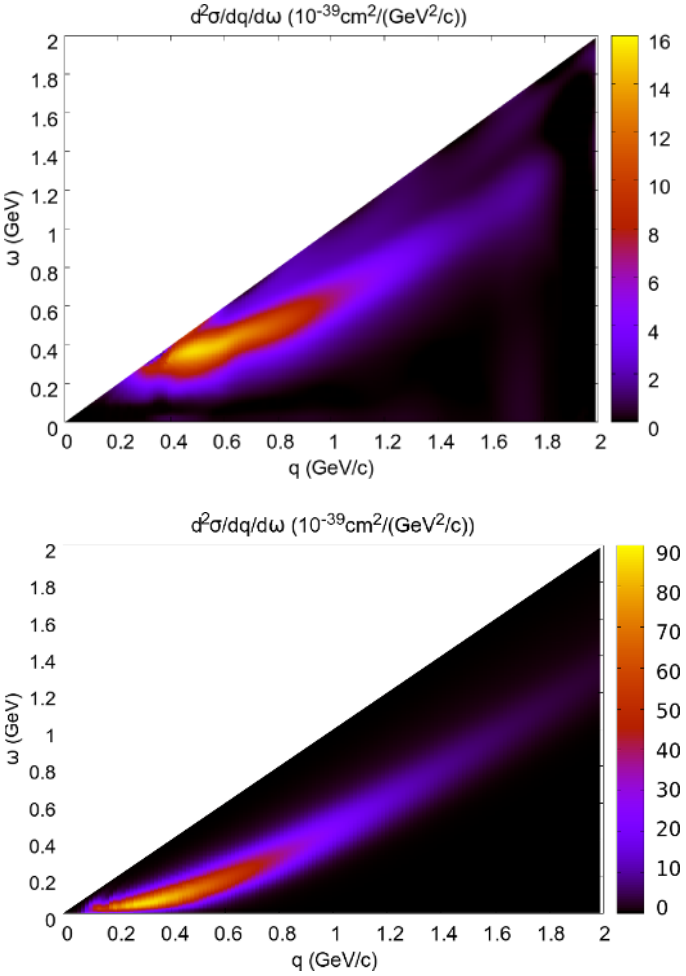

FIG. 4. (Color online) 2p-2h MEC (top panel) and QE (bottom panel) density plots of the double-differential cross section per neutron of ^{12}C versus ω and q at $E_\nu = 3$ GeV.

	$\tilde{f}_{L,T=1}$	$\tilde{f}_{L,T=0}$	$\tilde{f}_T$
β	0.8923	1.0361	0.9425
σ	0.6572	0.5817	0.7573
ψ_0	0.1708	0.02217	−0.4675
$1/\nu_0$	−0.7501	−0.1163	2.9381

TABLE I. Values of the parameters that characterize the RMF scaling functions.

Moreover, the reference RPWIA scaling functions are described as

$$\tilde{f}_{L,T}^{RPWIA} = \frac{2(a_3)_{L,T}}{1+\exp\left(\frac{\psi-a_1}{a_2}\right)} \exp\left(-\frac{(\psi-a_4)^2}{a_5}\right), \quad \text{(A5)}$$

with $a_1 = -0.892196$, $a_2 = 0.1792$, $(a_3)_L = 6070.85$, $(a_3)_T = 6475.57$, $a_4 = 1.74049$, $a_5 = 0.64559$. There are no significant differences associated to isospin effects (isovector, isoscalar) on the RPWIA scaling functions.

In order to reproduce the peak position of RMF and RPWIA scaling functions within SuSAv2 we consider a q-dependent energy shift, namely, $E_{shift}(q)$. This quantity modifies the scaling variable $\psi(q,\omega) \longrightarrow \psi'(q,\omega,E_{shift})$ as

$$\psi' = \frac{1}{\sqrt{\xi_F}} \frac{\lambda'-\tau'}{\sqrt{(1+\lambda')\tau' + \kappa\sqrt{\tau'(\tau'+1)}}} \quad \text{(A6)}$$

where $\xi_F = \sqrt{1+(k_F/M)^2} - 1$, $\kappa = q/(2M)$, $\lambda' = \omega'/(2M)$ and $\tau = \kappa^2 - \lambda'^2$. M is the nucleon mass and k_F is the Fermi momentum. Additionally, we have introduced the variable $\omega' = \omega - E_{shift}$.

In particular, we build this function $E_{shift}(q)$ from the results of the RMF and RPWIA models presented in [23]. In the particular case of ^{12}C, the energy shift for the longitudinal and transverse RMF/RPWIA scaling functions is defined (in GeV) as

$$\begin{aligned} E_{shift,L}^{RMF} &= -0.005506 + 0.0548 * q \\ E_{shift,T}^{RMF} &= -0.007687 + 0.0564 * q \\ E_{shift,L}^{RPWIA} &= 0.035164 + 0.0112 * q \\ E_{shift,T}^{RPWIA} &= -0.007687 + 0.0564 * 0.827 \end{aligned} \quad \text{(A7)}$$

Appendix B: RMF/RPWIA transition function

As described in the Introduction, a blending function is incorporated to the SuSAv2 model to account properly for the RMF and RPWIA contributions at the different kinematics. Although more information on this issue can be found on [14], the scaling functions are defined as a linear combination of RMF-based ($\tilde{f}_{L,T}^{RMF}$) and RPWIA ($f_{L,T}^{RPWIA}$) scaling functions,

$$\mathcal{F}_L^{T=0,1} \equiv \cos^2\chi(q)\tilde{f}_L^{T=0,1} + \sin^2\chi(q)\tilde{f}_L^{RPWIA}$$
$$\mathcal{F}_T \equiv \cos^2\chi(q)\tilde{f}_T + \sin^2\chi(q)\tilde{f}_T^{RPWIA}\,, \tag{B1}$$

where $\chi(q)$ is a q-dependent angle given by

$$\chi(q) \equiv \frac{\pi}{2}\left(1 - \left[1 + e^{\left(\frac{(q-q_0)}{\omega_0}\right)}\right]^{-1}\right) \tag{B2}$$

and the transition between RMF and RPWIA behaviors occurs at intermediate q-values (q_0) in a region of width ω_0, which is fixed at 200 MeV.

The behaviour of the q_0 parameter is analyzed in detail in [14] where the following parametrization is suggested

$$q_0(q) = \begin{cases} A + Bq, & q < q_1 \\ C + Dq, & q > q_1 \end{cases} \tag{B3}$$

with $q_1 = 700$MeV/c, $A = 377.629$ MeV/c, $B = 0.407$, $C = -5.322$ MeV/c and $D = 0.968$.

[1] A. A. Aguilar-Arevalo *et al.* (MiniBooNE Collaboration), Phys. Rev. D **81**, 092005 (2010).
[2] A. A. Aguilar-Arevalo *et al.* (MiniBooNE Collaboration), Phys. Rev. D **88**, 032001 (2013).
[3] V. Lyubushkin *et al.* (NOMAD Collaboration), Eur. Phys. J. C **63**, 355 (2009).
[4] K. Abe *et al.* (T2K Collaboration), Phys. Rev. D **87**, 092003 (2013).
[5] K. Abe *et al.* (T2K Collaboration), Phys. Rev. Lett. **113**, 241803 (2014).
[6] K. Abe *et al.* (T2K Collaboration), Phys. Rev. D **93**, 112012 (2016).
[7] Y. Nakajima *et al.* (SciBooNE Collaboration), Phys. Rev. D **83**, 012005 (2011).
[8] G. A. Fiorentini *et al.* (MINERνA collaboration), Phys. Rev. Lett. **111**, 022502 (2013).
[9] L. Fields *et al.* (MINERνA collaboration), Phys. Rev. Lett. **111**, 022501 (2013).
[10] M. Martini, M. Ericson, G. Chanfray, and J. Marteau, Phys. Rev. C **80**, 065501 (2009).
[11] J. E. Amaro, M. B. Barbaro, J. A. Caballero, T. W. Donnelly, and C. F. Williamson, Phys. Lett. B **696**, 151 (2011).
[12] J. Nieves, I. Ruiz Simo, and M. J. Vicente Vacas, Phys. Lett. B **707**, 72 (2012).
[13] O. Lalakulich, K. Gallmeister, and U. Mosel, Phys. Rev. C **86**, 014614 (2012).
[14] G. D. Megias, J. E. Amaro, M. B. Barbaro, J. A. Caballero, and T. W. Donnelly, Phys. Rev. D **94**, 013012 (2016).
[15] D. B. Day, J. S. McCarthy, T. W. Donnelly, and I. Sick, Annu. Rev. Nucl. Part. Sci. **40**, 357 (1990).
[16] T. W. Donnelly and I. Sick, Phys. Rev. Lett. **82**, 3212 (1999).
[17] T. W. Donnelly and I. Sick, Phys. Rev. C **60**, 065502 (1999).
[18] J. E. Amaro, M. B. Barbaro, J. A. Caballero, T. W. Donnelly, A. Molinari, and I. Sick, Phys. Rev. C **71**, 015501 (2005).
[19] C. Maieron, T. W. Donnelly, and I. Sick, Phys. Rev. C **65**, 025502 (2002).
[20] M. B. Barbaro, J. A. Caballero, T. W. Donnelly, and C. Maieron, Phys. Rev. C **69**, 035502 (2004).
[21] C. Maieron, J. E. Amaro, M. B. Barbaro, J. A. Caballero, T. W. Donnelly, and C. F. Williamson, Phys. Rev. C **80**, 035504 (2009).
[22] M. V. Ivanov, G. D. Megias, R. González-Jiménez, O. Moreno, M. B. Barbaro, J. A. Caballero, and T. W. Donnelly, J. Phys. G **43**, 045101 (2016).
[23] R. González-Jiménez, G. D. Megias, M. B. Barbaro, J. A. Caballero, and T. W. Donnelly, Phys. Rev. C **90**, 035501 (2014).
[24] J. A. Caballero, J. E. Amaro, M. B. Barbaro, T. W. Donnelly, C. Maieron, and J. M. Udías, Phys. Rev. Lett. **95**, 252502 (2005).
[25] J. A. Caballero, Phys. Rev. C **74**, 015502 (2006).
[26] J. A. Caballero, J. E. Amaro, M. B. Barbaro, T. W. Donnelly, and J. M. Udías, Phys. Lett. B **653**, 366 (2007).
[27] G. D. Megias, T. W. Donnelly, O. Moreno, C. F. Williamson, J. A. Caballero, R. González-Jiménez, A. De Pace, M. B. Barbaro, W. M. Alberico, M. Nardi, and J. E. Amaro, Phys. Rev. D **91**, 073004 (2015).
[28] A. De Pace, M. Nardi, W. M. Alberico, T. W. Donnelly, and A. Molinari, Nucl. Phys. A **726**, 303 (2003).
[29] A. De Pace, M. Nardi, W. M. Alberico, T. W. Donnelly, and A. Molinari, Nucl. Phys. A **741**, 249 (2004).
[30] I. Ruiz Simo, C. Albertus, J. E. Amaro, M. B. Barbaro, J. A. Caballero, and T. W. Donnelly, Phys. Rev. D **90**, 033012 (2014).
[31] I. Ruiz Simo, J. E. Amaro, M. B. Barbaro, J. A. Caballero, A. De Pace, and T. W. Donnelly, arXiv:1604.08423 [nucl-th].
[32] I. Ruiz Simo, J. E. Amaro, M. B. Barbaro, J. A. Caballero, G. D. Megias, A. De Pace, and T. W. Donnelly, arXiv:1606.06480 [nucl-th].
[33] J. E. Amaro, M. B. Barbaro, J. A. Caballero, T. W. Donnelly, and C. Maieron, Phys. Rev. C **71**, 065501 (2005).
[34] M. Martini, M. Ericson, and G. Chanfray, Phys. Rev. C **84**, 055502 (2011).
[35] M. J. Dekker, P. J. Brussaard, and J. A. Tjon, Phys. Rev. **C49**, 2650 (1994).
[36] O. Benhar, A. Lovato, and N. Rocco, Phys. Rev. **C92**, 024602 (2015).
[37] J. Nieves, I. Ruiz Simo, and M. J. Vicente Vacas, Phys. Rev. C **83**, 045501 (2011).
[38] A. Lovato, S. Gandolfi, J. Carlson, S. C. Pieper, and R. Schiavilla, Phys. Rev. Lett. **117**, 082501 (2016).
[39] A. Lovato, S. Gandolfi, J. Carlson, S. C. Pieper, and R. Schiavilla, Phys. Rev. **C91**, 062501 (2015).
[40] J. E. Amaro, A. M. Lallena, and G. Co, Nucl. Phys. **A578**, 365 (1994).
[41] R. Gran, J. Nieves, F. Sánchez, and M. J. Vicente Vacas,

Phys. Rev. D **88**, 113007 (2013).
[42] A. Gil, J. Nieves, and E. Oset, Nucl. Phys. **A627**, 543 (1997).
[43] M. Martini, M. Ericson, and G. Chanfray, Phys. Rev. D **85**, 093012 (2012).
[44] K. McFarland, Private communication.
[45] J. Wolcott *et al.* (MINERνA collaboration), Phys. Rev. Lett. **116**, 081802 (2016).
[46] G. D. Megias, M. V. Ivanov, R. González-Jiménez, M. B. Barbaro, J. A. Caballero, T. W. Donnelly, and J. M. Udías, Phys. Rev. D **89**, 093002 (2014).
[47] V. Pandey, N. Jachowicz, M. Martini, R. González-Jiménez, J. Ryckebusch, T. Van Cuyck, and N. Van Dessel, arXiv:1607.01216 [nucl-th].
[48] K. Gallmeister, U. Mosel, and J. Weil, arXiv:1605.09391 [nucl-th].
[49] I. Ruiz Simo, J. E. Amaro, M. B. Barbaro, A. De Pace, J. A. Caballero, G. D. Megias, and T. W. Donnelly, Phys. Lett. **B762**, 124 (2016).

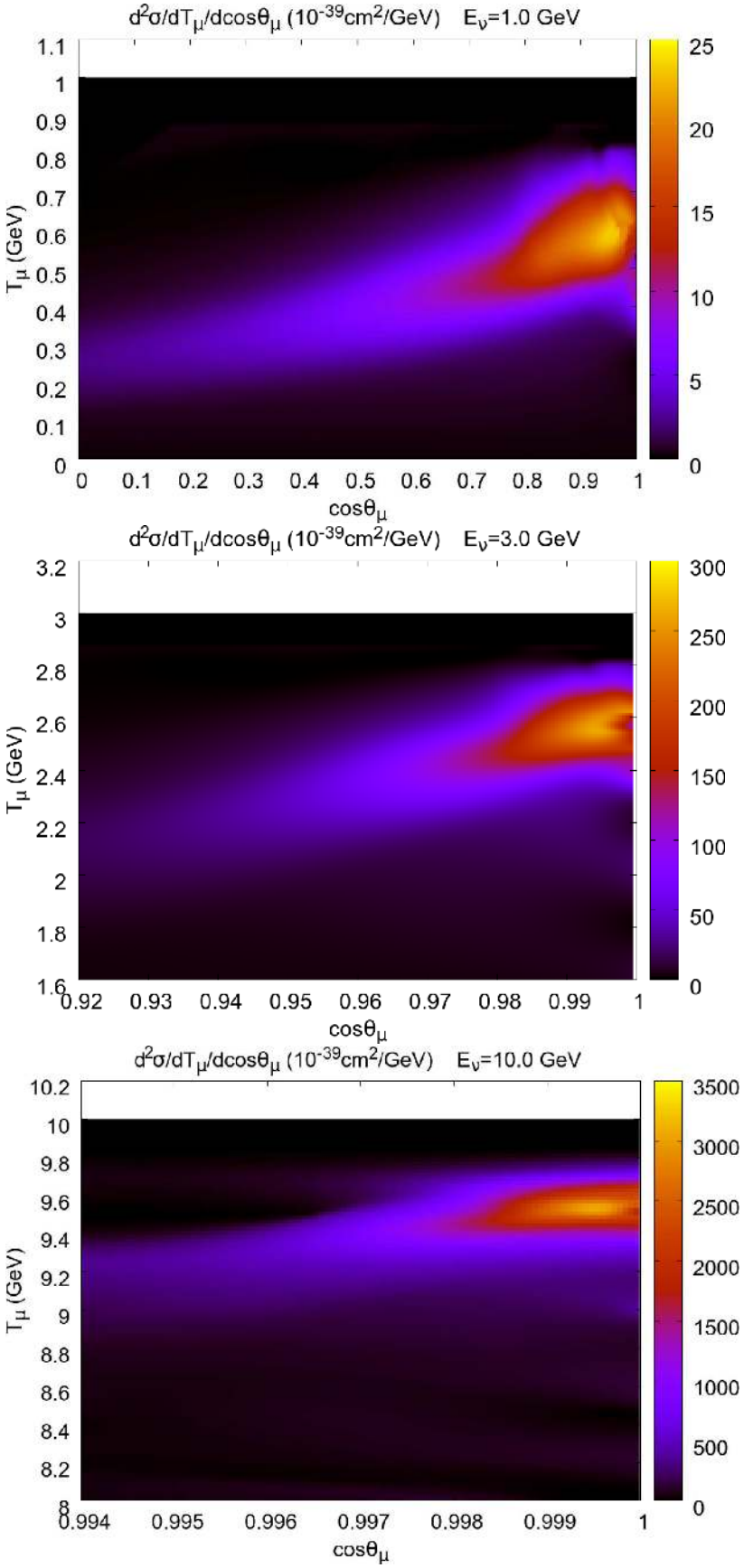

FIG. 5. (Color online) 2p-2h MEC density plots of the double-differential cross section per neutron of ^{12}C at three different neutrino energies E_ν versus T_μ and $\cos\theta_\mu$.

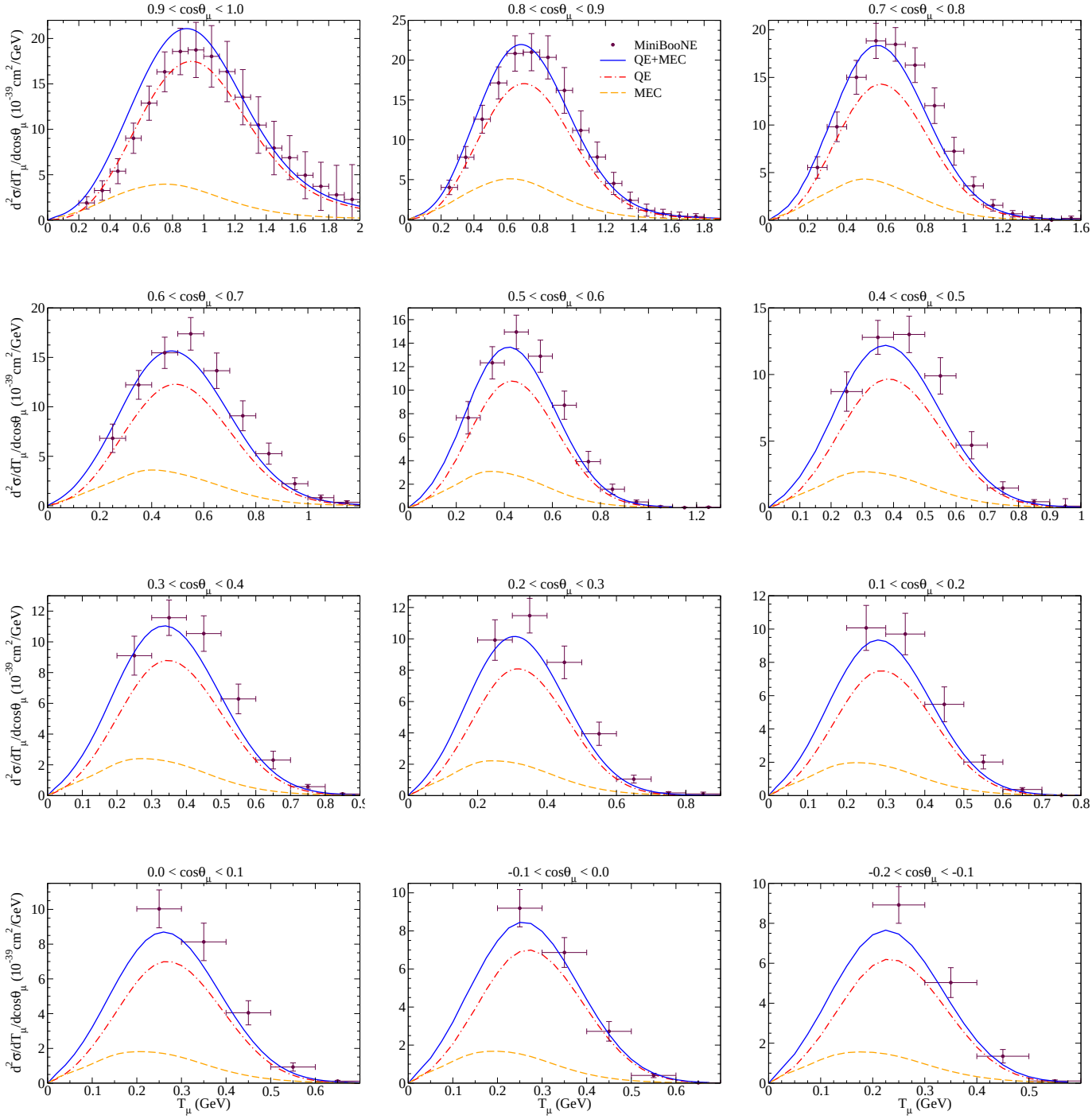

FIG. 6. (Color online) MiniBoone flux-folded double differential cross section per target nucleon for the ν_μ CCQE process on ^{12}C displayed versus the μ^- kinetic energy T_μ for various bins of $\cos\theta_\mu$ obtained within the SuSAv2+MEC approach. QE and 2p-2h MEC results are also shown separately. Data are from [1].

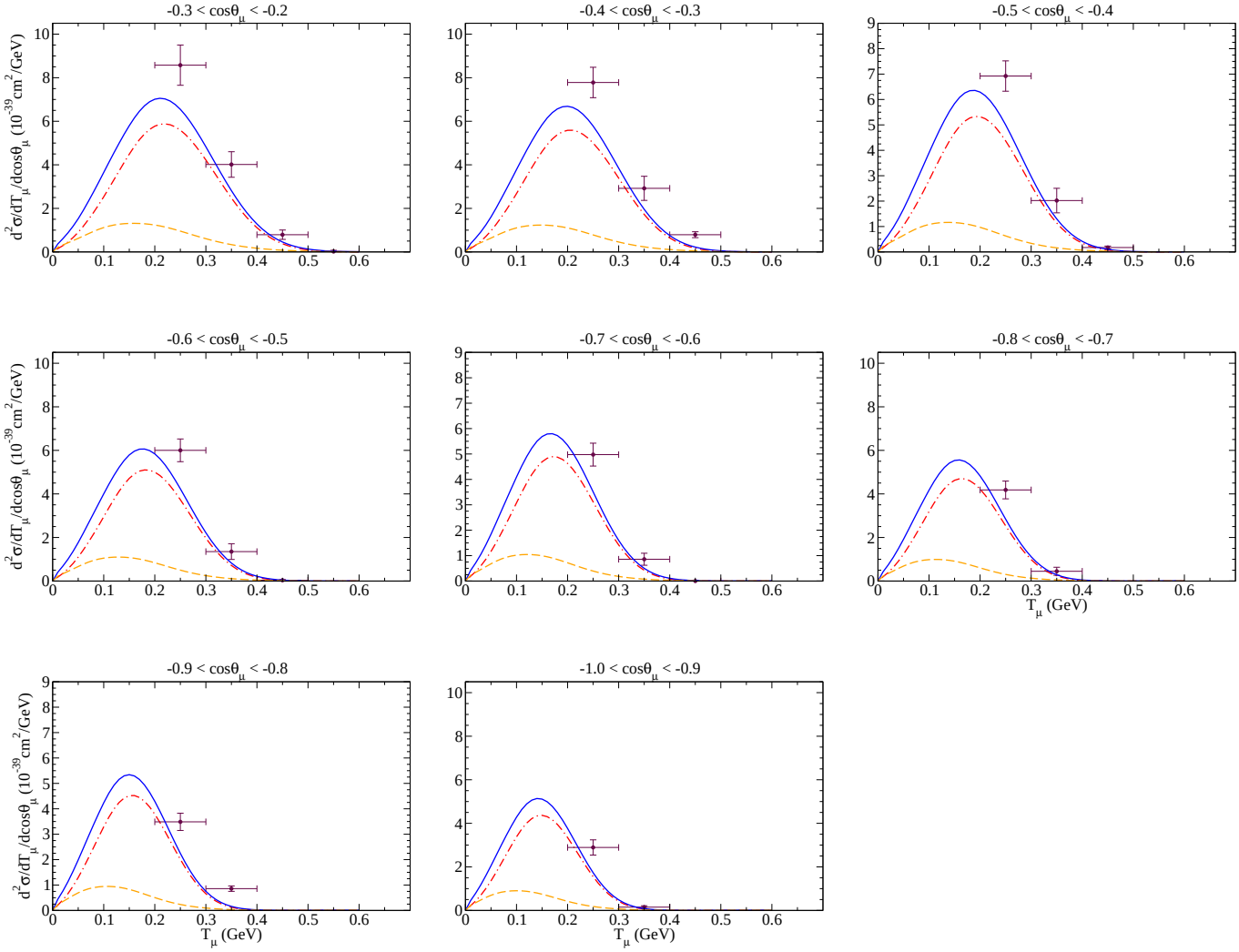

FIG. 7. (Color online) As for Fig. 6 but considering more backward kinematics. Data are from [1].

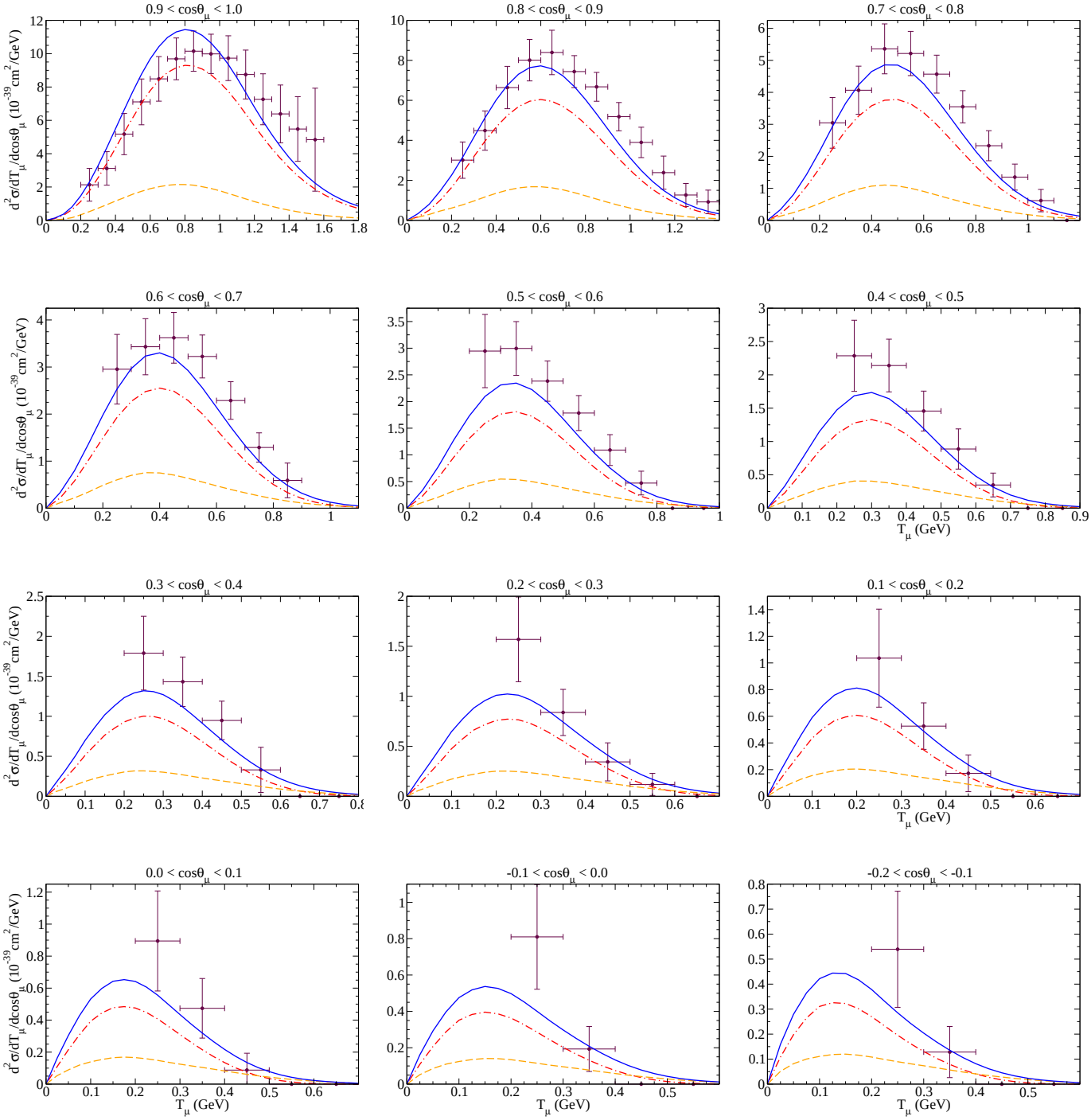

FIG. 8. (Color online) As for Fig. 6, but now for the $\bar{\nu}_\mu$ CCQE process on ^{12}C. Data are from [2].

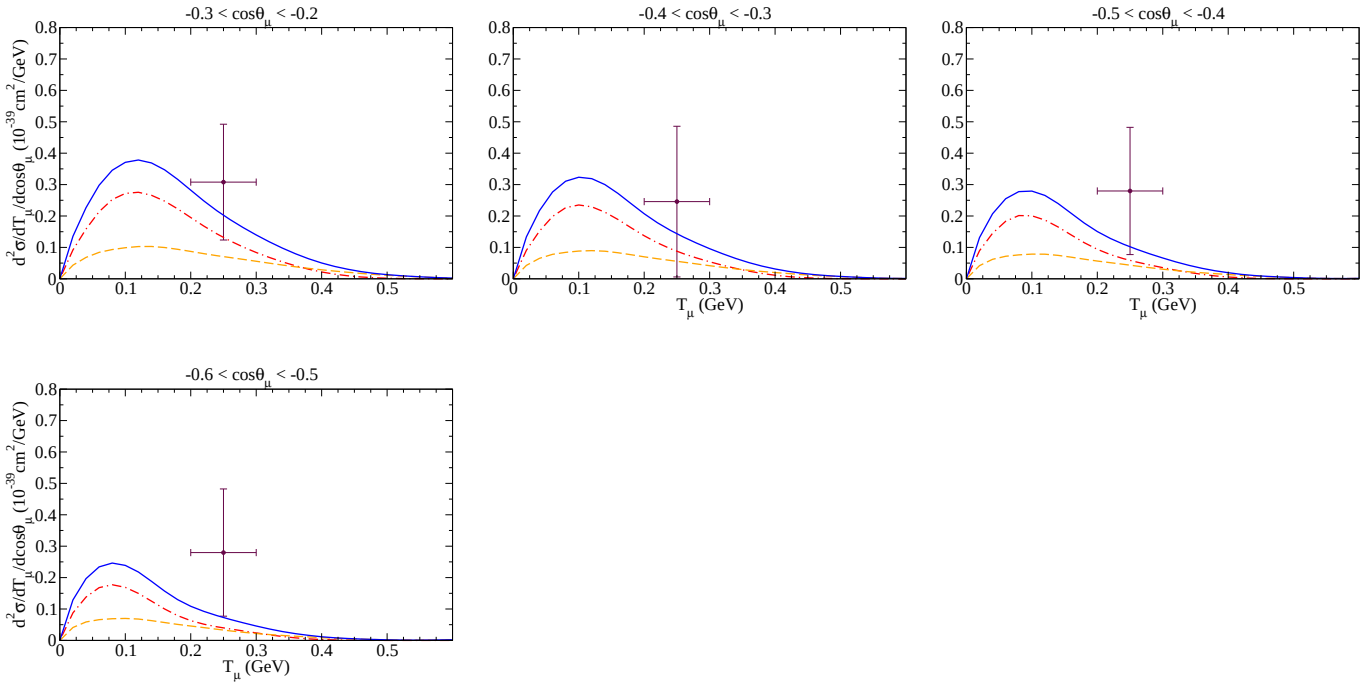

FIG. 9. (Color online) As for Fig. 8, but considering more backward kinematics. Data are from [2].

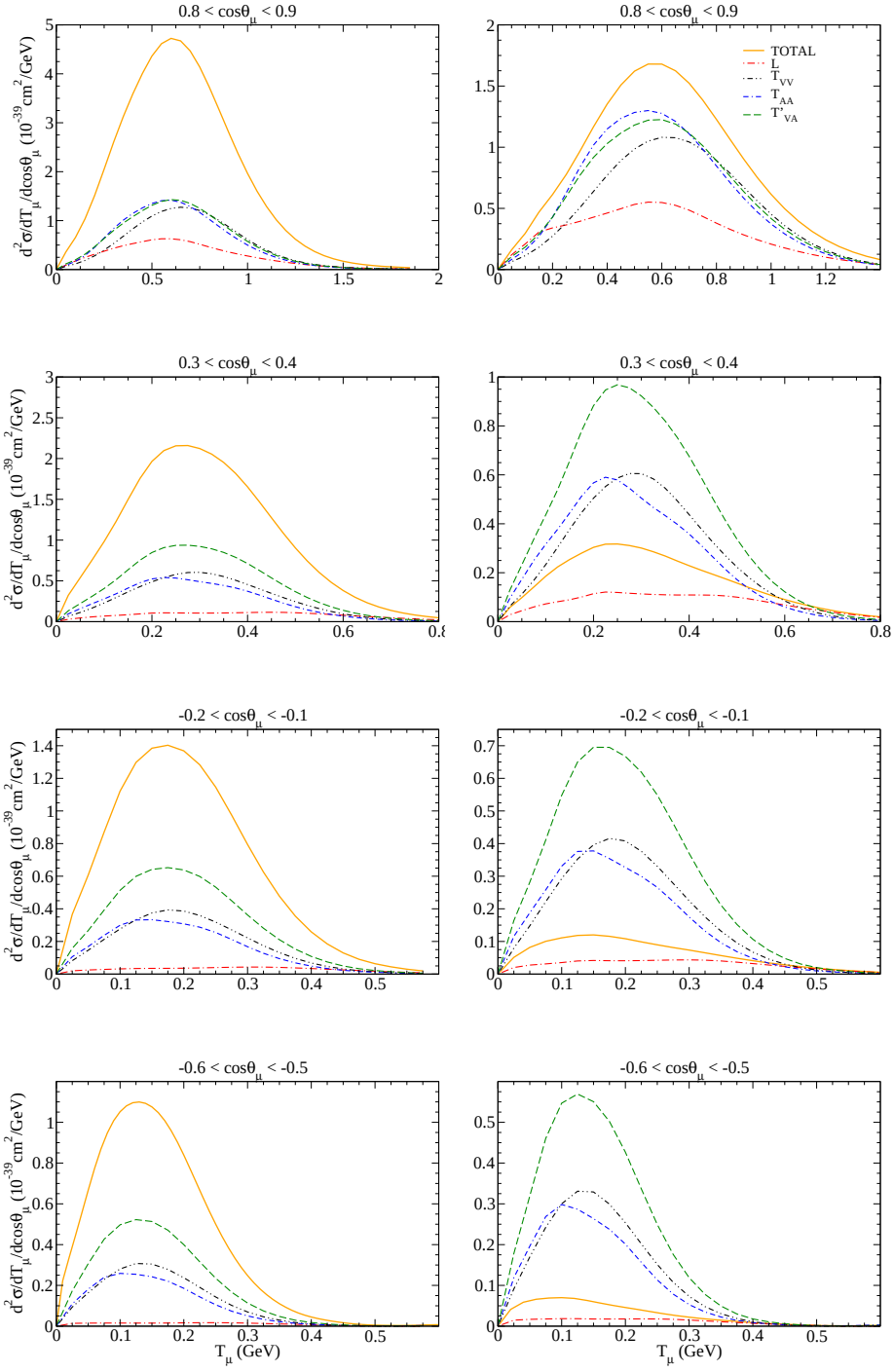

FIG. 10. (Color online) Comparison of the different 2p-2h MEC channels for the ν_μ (left panels) and $\bar{\nu}_\mu$ (right panels) MiniBooNE double differential cross section.

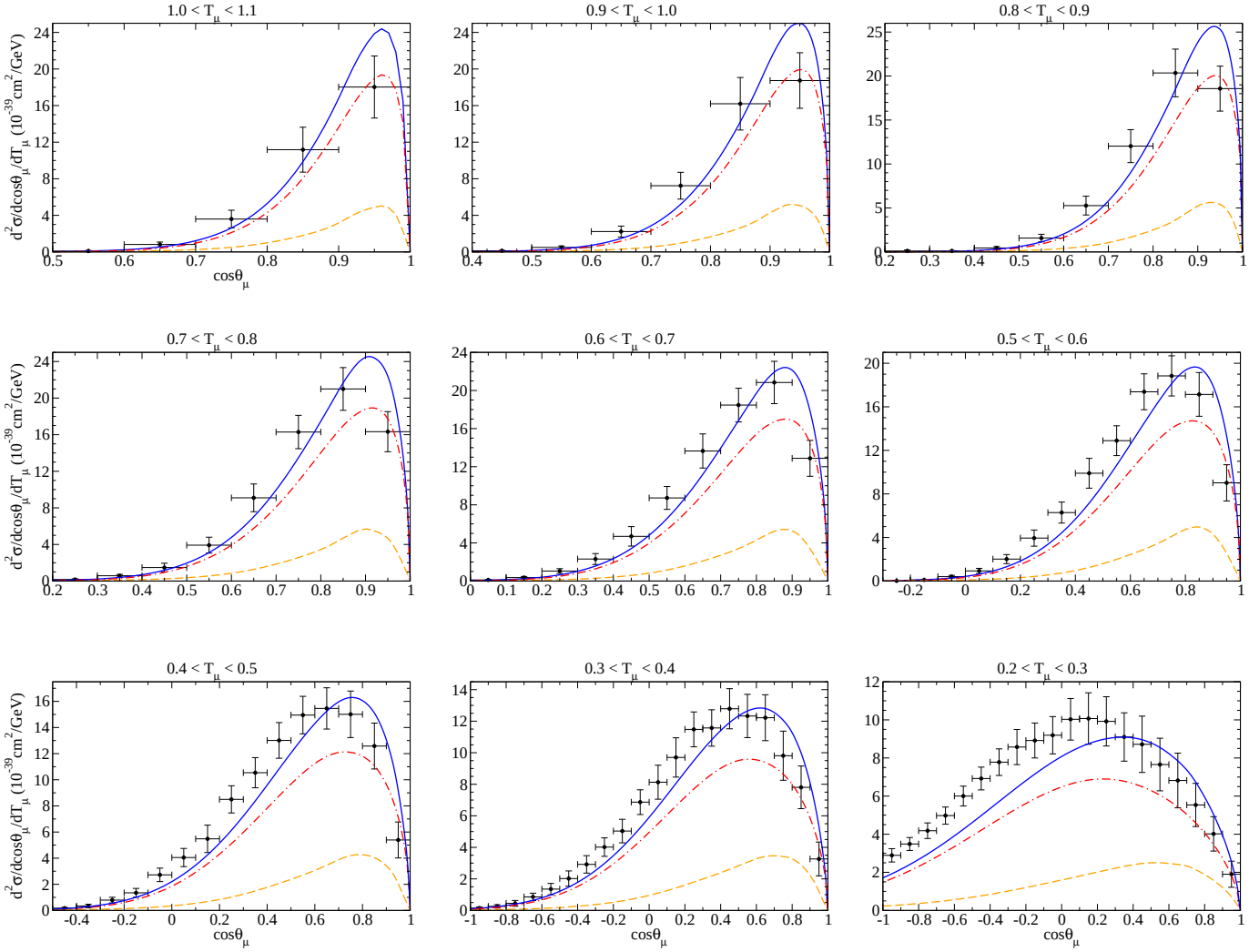

FIG. 11. (Color online) MiniBoone flux-folded double differential cross section per target nucleon for the ν_μ CCQE process on ^{12}C displayed versus $\cos\theta_\mu$ for various bins of T_μ obtained within the SuSAv2+MEC approach. QE and 2p-2h MEC results are also shown separately. Data are from [1].

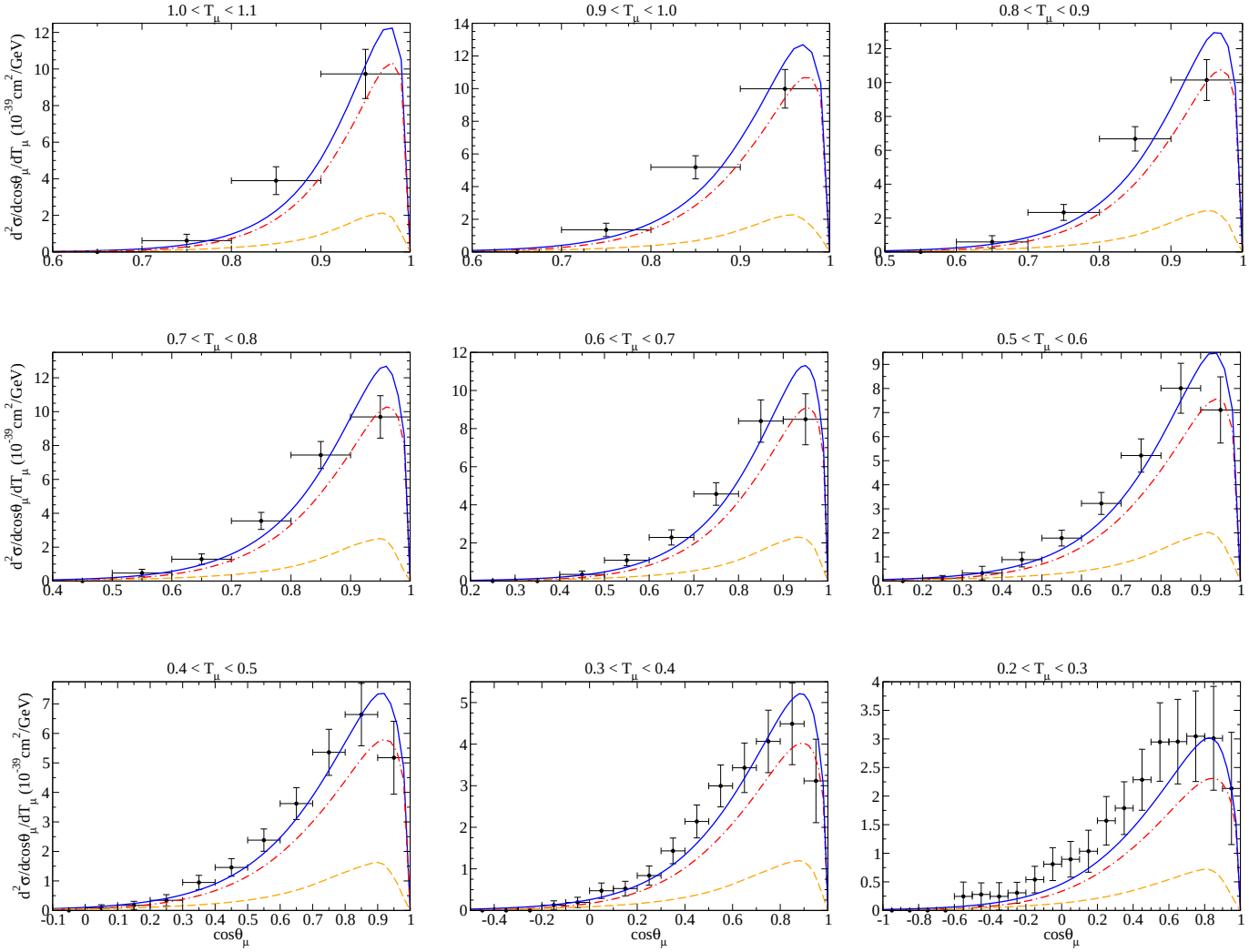

FIG. 12. (Color online) As for Fig. 11, but now for the $\bar{\nu}_\mu$ CCQE process on ^{12}C. Data are from [2].

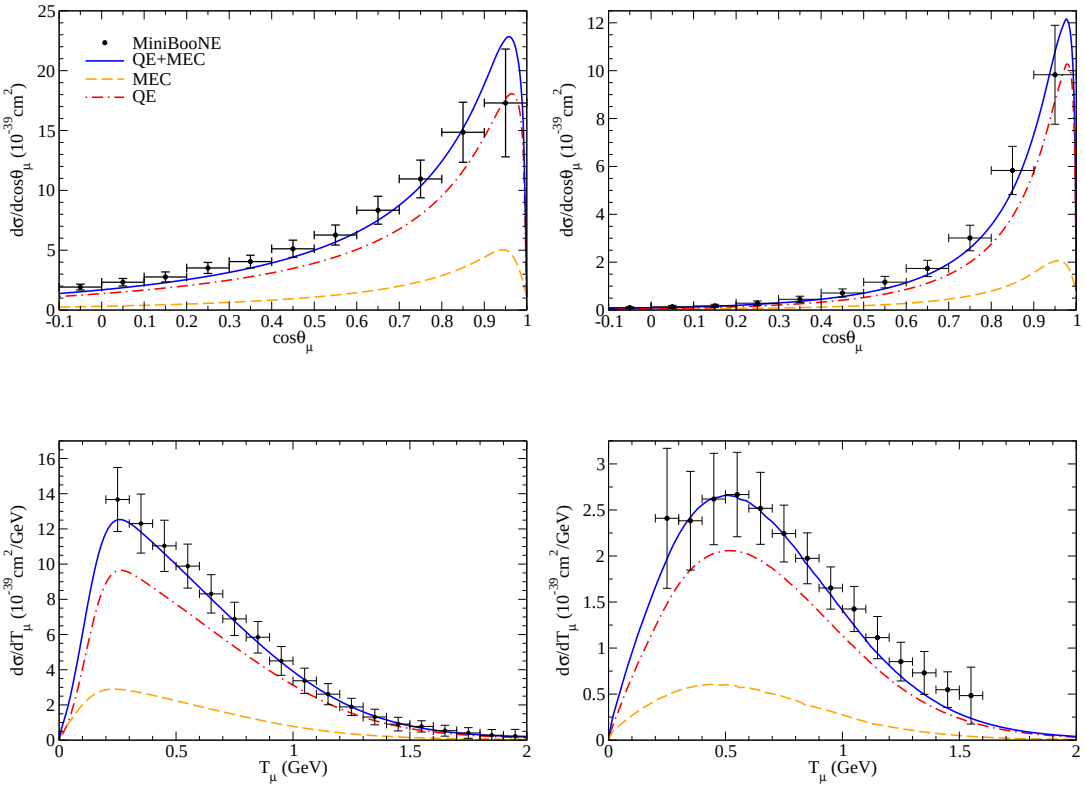

FIG. 13. (Color online) MiniBooNE flux-averaged CCQE ν_μ-^{12}C ($\bar{\nu}_\mu$-^{12}C) differential cross section per nucleon as a function of the muon scattering angle (top panels) and of the muon kinetic energy (bottom panels). The left panels correspond to neutrino cross sections and the right ones to antineutrino reactions. Data are from [1, 2]

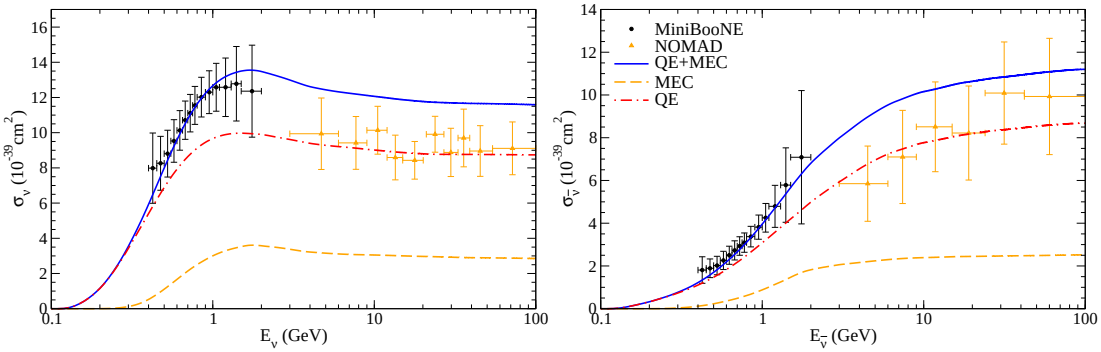

FIG. 14. (Color online) MiniBooNE CCQE ν_μ-^{12}C ($\bar{\nu}_\mu$-^{12}C) total cross section per nucleon as a function of the neutrino energy. The left panel correspond to neutrino cross sections and the right one to antineutrino reactions. Data are from [1, 2]

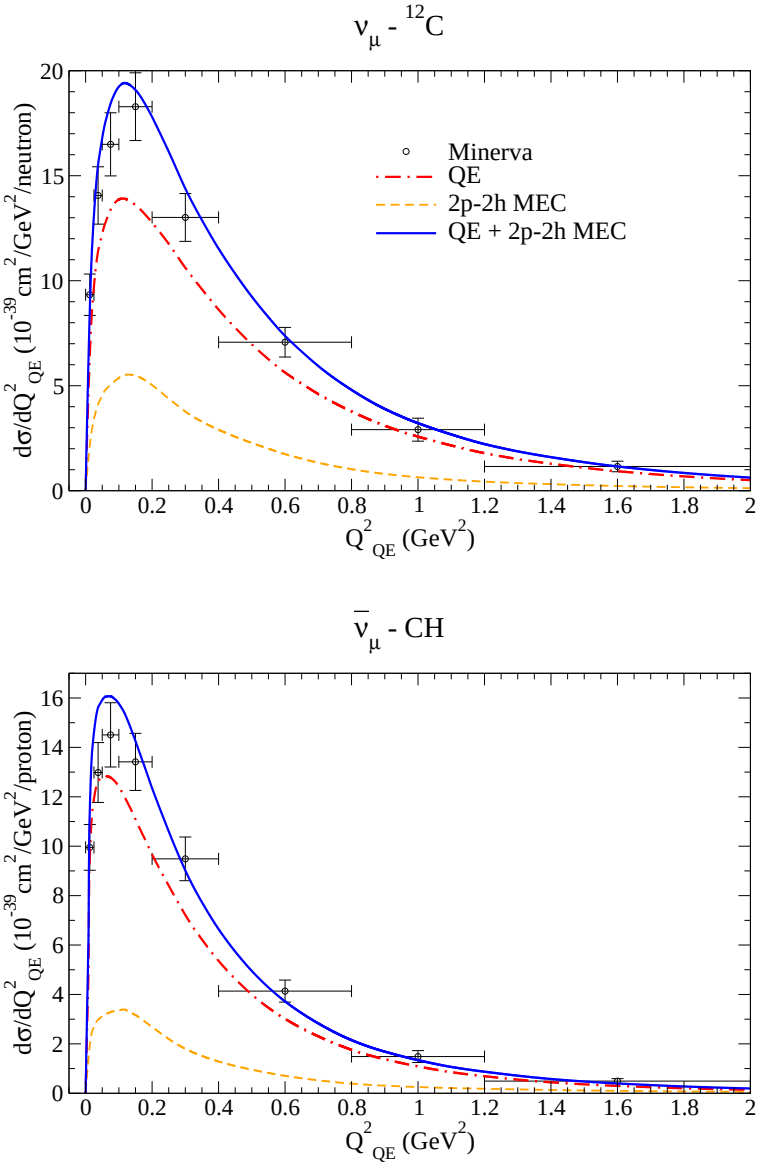

FIG. 15. (Color online) Flux-folded $\nu_\mu - ^{12}$C CCQE (upper panel) and $\bar{\nu}_\mu$−CH (lower panel) scattering cross section per target nucleon as a function of Q^2_{QE} and evaluated in the SuSAv2 and SuSAv2+MEC models. MINERνA data are from [44].

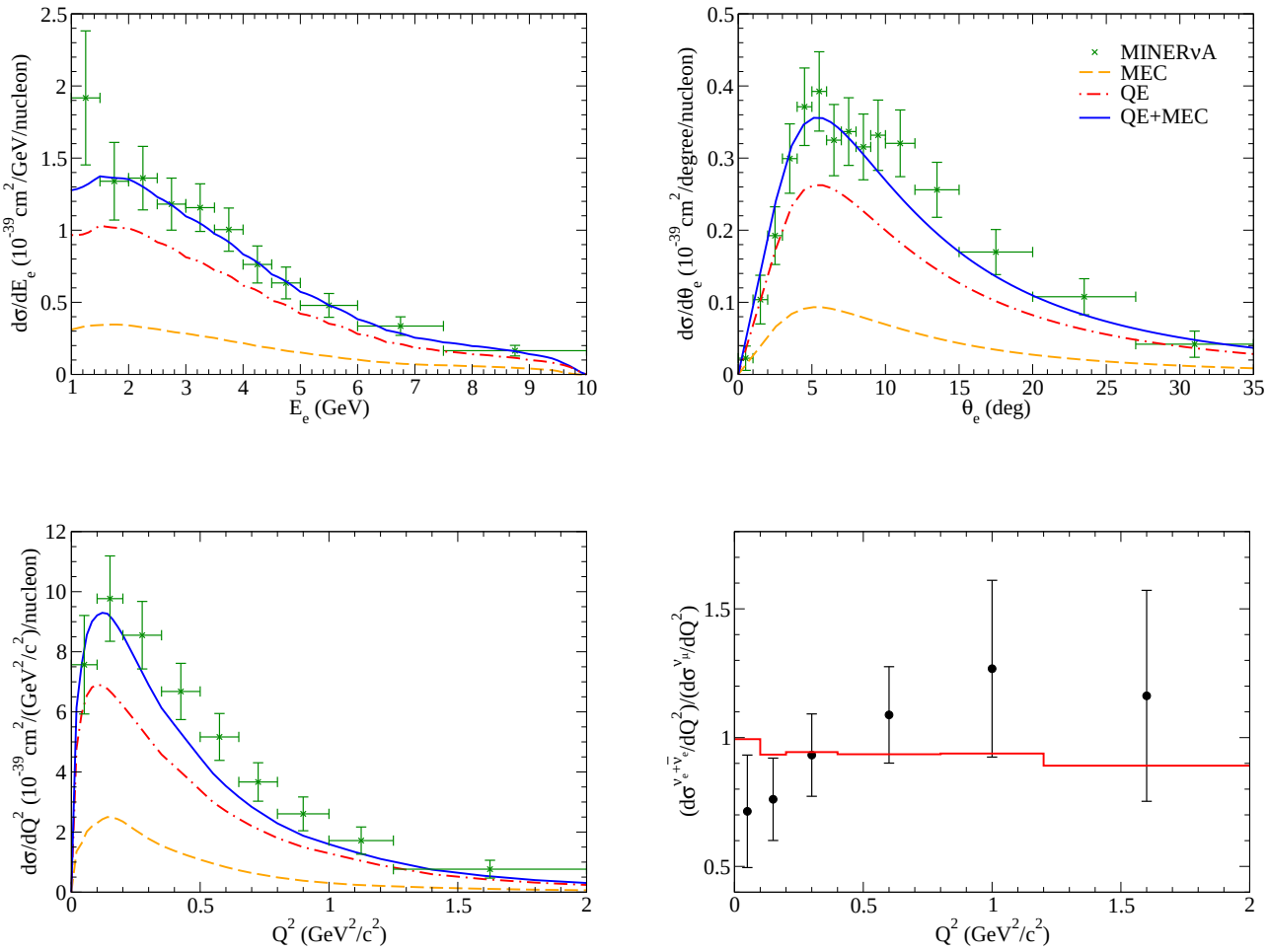

FIG. 16. (Color online) MINERνA flux-integrated differential ν_e CCQE-like cross section vs. electron energy (top left) and electron angle (top right). The cross section vs. Q^2_{QE} is shown in the bottom panel. Data are from [45].

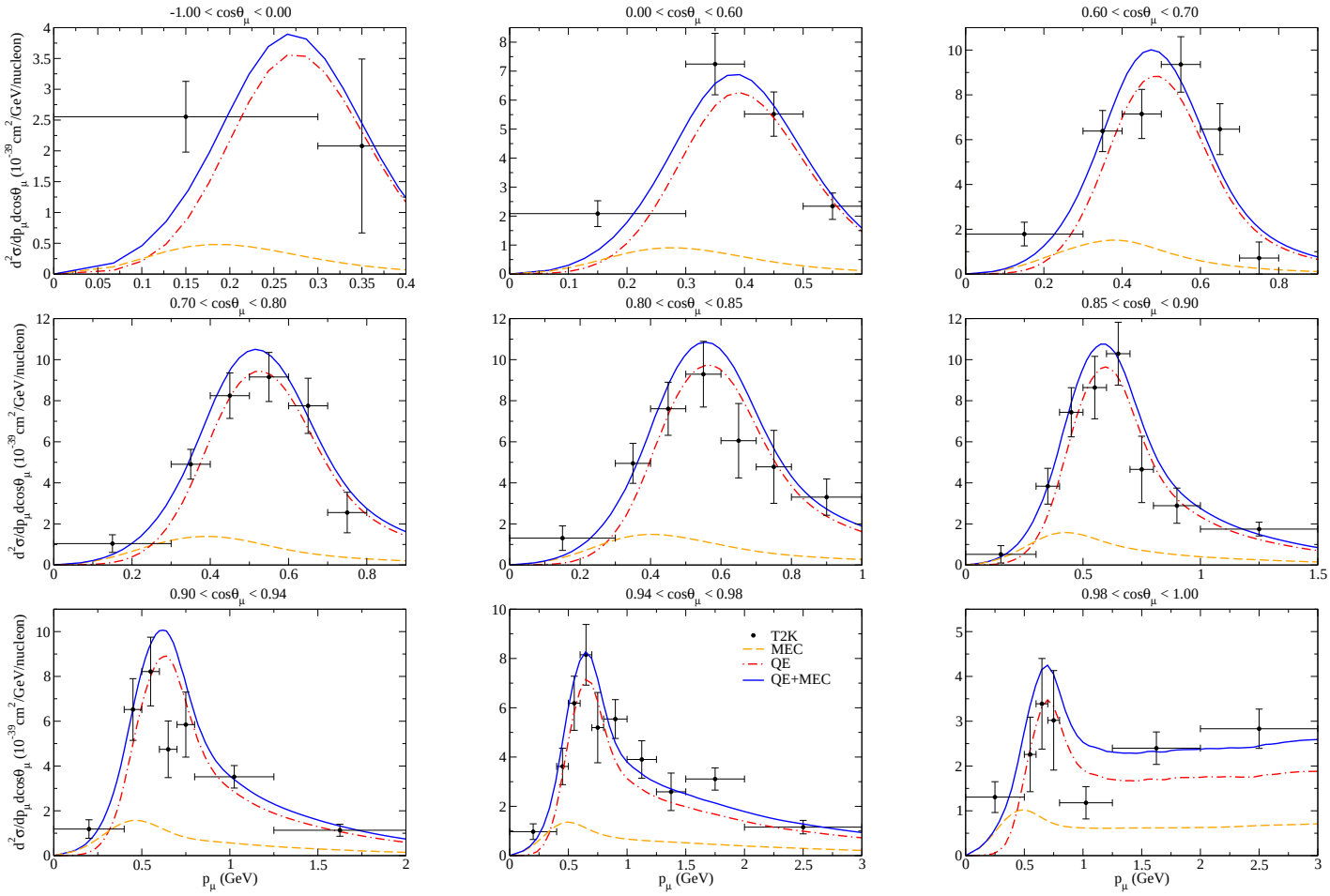

FIG. 17. (Color online) T2K flux-folded double differential cross section per target nucleon for the ν_μ CCQE process on ^{12}C displayed versus the μ^- momentum p_μ for various bins of $\cos\theta_\mu$ obtained within the SuSAv2+MEC approach. QE and 2p-2h MEC results are also shown separately. Data are from [6].

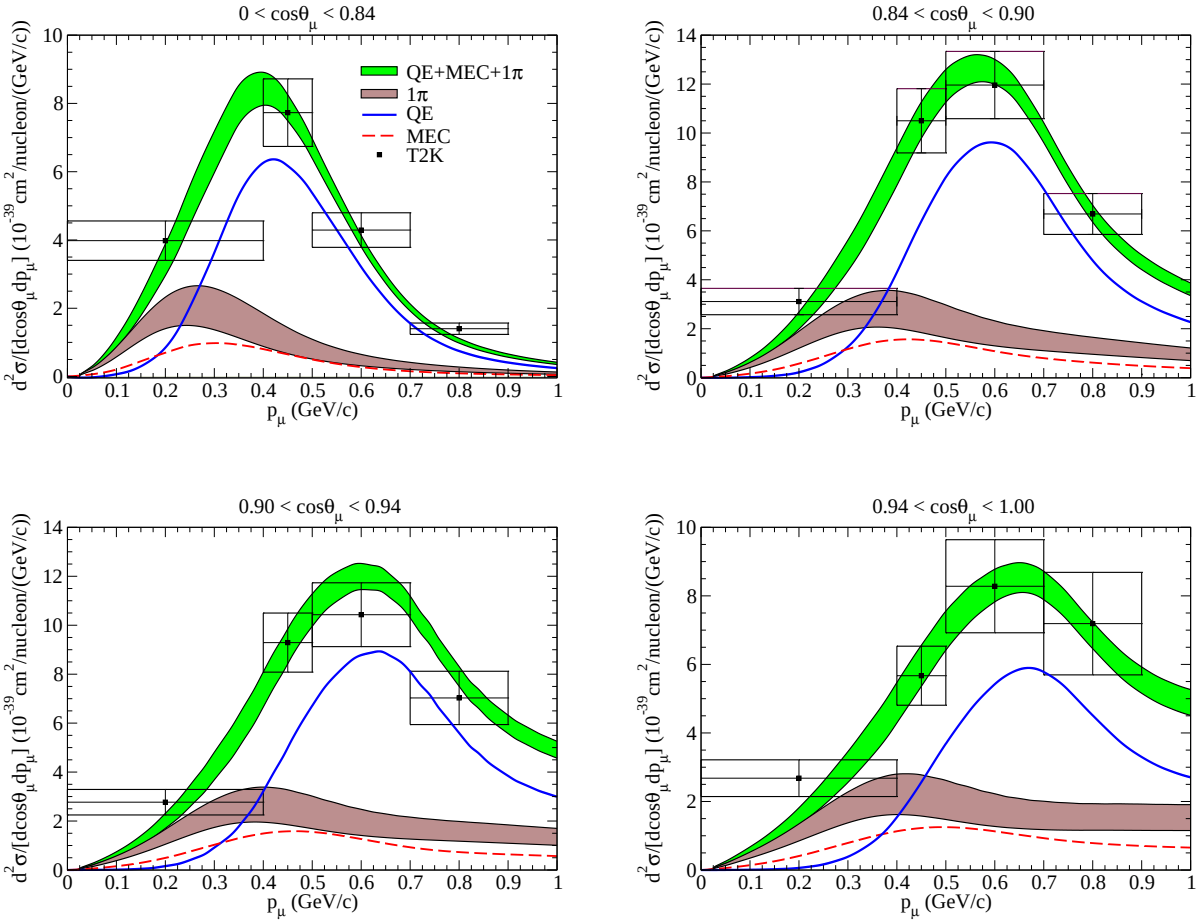

FIG. 18. (Color online) The CC-inclusive T2K flux-folded $\nu_\mu - {}^{12}$C double-differential cross section per nucleon evaluated in the SuSAv2+MEC model is displayed as a function of the muon momentum for different bins in the muon angle. The separate contributions of the QE, 1π and 2p-2h MEC are displayed. The data are from [4]

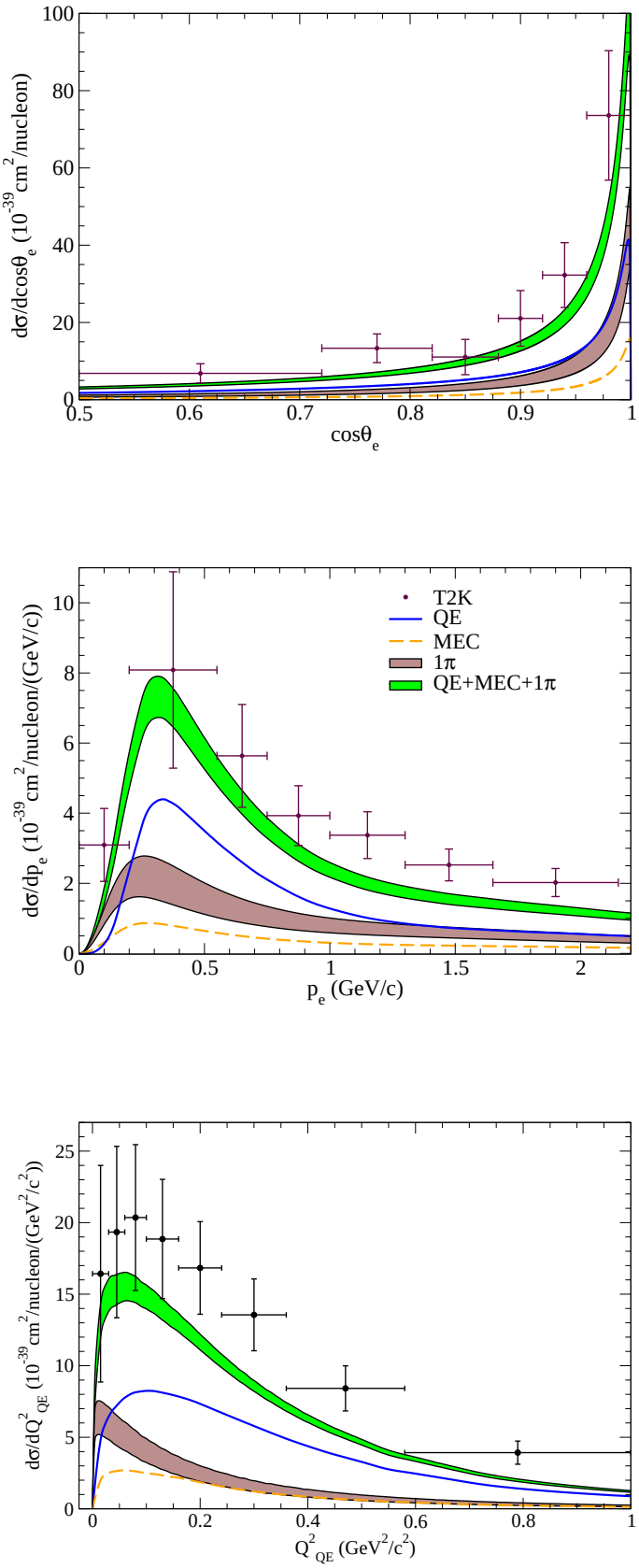

FIG. 19. (Color online) The CC-inclusive T2K flux-folded $\nu_e - {}^{12}$C differential cross section per nucleon evaluated in the SuSAv2+MEC model is displayed as a function of the electron momentum (top), $\cos\theta_e$ (middle) and Q^2_{QE} (bottom). The separate contributions of the QE, 1π and 2p-2h MEC are displayed. The data are from [5].

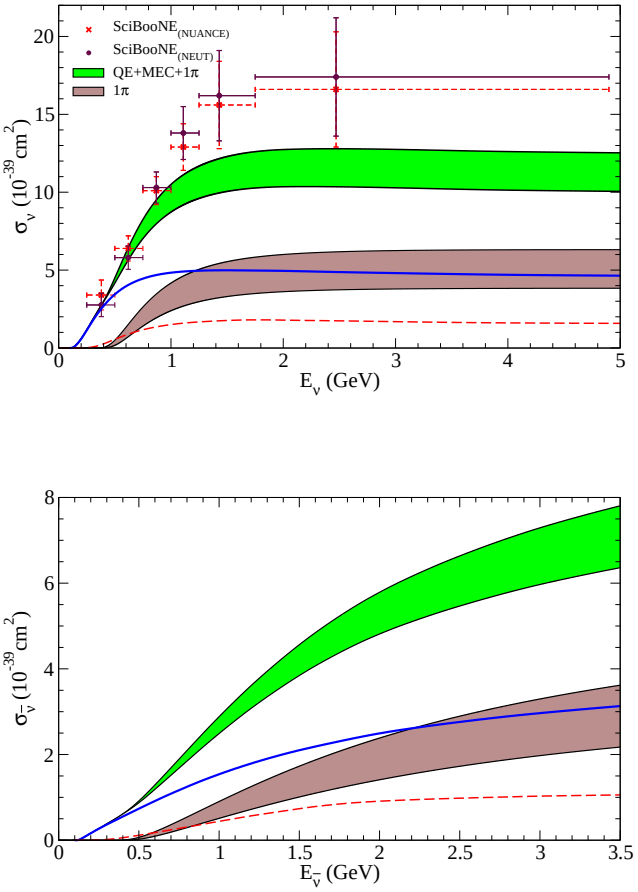

FIG. 20. (Color online) The CC-inclusive ν_μ (left) and $\bar{\nu}_\mu$ (right) cross section on a polystyrene target (C_8H_8) per nucleon evaluated in the SuSAv2+MEC model as a function of the neutrino energy. The SciBooNE data are from [7].